Department of Physics and Astronomy

University of Heidelberg

Master Thesis in Physics

submitted in 2020

by Michael Quin

born in Portadown,

United Kingdom

Coherence Effects

and Spin Polarisation

of Electrons in Electromagnetic Fields

This Master thesis has been carried out by Michael Quin

at the

Max Planck Institute for Nuclear Physics

under the supervision of

Priv.-Doz. Dr. Antonino Di Piazza

and Dr. Matteo Tamburini

Kohärenzeffekte und Spinpolarisation von Elektronen in Elektromagnetischen Feldern:

Die Kollision relativistischer Elektronen mit einem sich gegenläufig ausbreitenden Laserpuls hat das Potenzial kurze Pulse von Harmonischen im Röntgenbereich zu erzeugen, die die molekulare, atomare und subatomare Dynamik verfolgen können. Auch die Erzeugung relativistischer, spinpolarisierter Elektronenstrahlen ist für die Untersuchung spinabhängiger, fundamentaler Wechselwirkungen in der Teilchenphysik von wesentlicher Bedeutung. Unser Ziel ist es, einen numerischen Code zu erstellen, der die Elektronen-Spin-Präzession modellieren und gleichzeitig das Spektrum und die Winkelverteilung der Energie, die von einer beliebigen Anzahl relativistischer und im Rahmen der klassischen Elektrodynamik mit einem externen Feld wechselwirkenden Elektronen emittiert wird, vorhersagen kann. Dieser Code wird streng gegen analytische Lösungen getestet. Mit numerischen und analytischen Ergebnissen können wir die Bedingungen für die Elektronenverteilung, die zur Erzeugung kohärenter Röntgenstrahlen erforderlich sind, und für spinpolarisierter Elektronenstrahlen untersuchen.

Coherence Effects and Spin Polarisation of Electrons in Electromagnetic Fields:

The collision of relativistic electrons with a counter propagating laser pulse can potentially generate short pulses of harmonics in the X-ray range, capable of tracking molecular, atomic and sub-atomic dynamics. Also, the creation of relativistic spin polarised electron beams is essential for probing spin dependent, fundamental interactions in particle physics. Our aim is to create a numerical code capable of modelling electron spin precession, while also predicting the spectrum and angular distribution of energy emitted from an arbitrary number of relativistic electrons, interacting with an external field in the domain of classical electrodynamics. This code will be rigorously tested against analytic solutions. With both numerical and analytic results, we can explore the conditions on the electron distribution necessary for generating coherent X-rays, and spin polarised electron beams.

Contents

Chapter 1

Introduction

The generation of short, coherent X-ray pulses has long been a goal of experimental physics due to the restriction of most lasers to optical wavelengths. Historically X-ray pulses have been obtained by synchrotron radiation, and are typically limited to picosecond duration. With the advent of free electron lasers, such as the Linac Coherent Light Source [LCL] and the European X-ray Free-Electron Laser Facility [XFE], we can generate femtosecond pulses with photon energies in the order of 10 keV [Emm+10; Ama+12]. These facilities produce X-rays by passing a relativistic electron beam from a linear accelerator through an alternating series of magnets known as an undulator. When the electrons are bunched together longitudinally their emitted radiation becomes coherent, and the frequency emitted can be tuned with the electron momentum or properties of the undulator. Alternatively, one can create a plasma with relativistically oscillating electrons by irradiating a solid or gas with an intense laser pulse. This process, known as high harmonic generation, is capable of producing attosecond pulses with photon energies in the order of $\lesssim 1$ keV [Kl09; Kor+18; Dro+06]. Without the need for a linear accelerator, this technique is compact. There are a wide range of applications for short X-ray pulses in crystallography [Wie+18], quantum optics [Ada+13], observing molecular, atomic and sub-atomic dynamics [Sin+16], with various medical applications [Col+16; Neu+00; Edw+94]. Throughout this thesis we will focus on a rival scheme for generating coherent X-rays, based on the collision of relativistic electrons with a counter propagating laser pulse. The change in frequency and amplitude of the reflected light can be described by the Doppler effect, as originally proposed by Einstein in his 1905 paper on Special Relativity [Ein05].

Laser-electron interactions are often parameterised in terms of the dimensionless wave amplitude $a_0 = eE_0/m_e c\omega_0$, for an electric field of amplitude E_0 and frequency ω_0, and an electron of charge $-e$ and mass m_e. For weak fields $a_0 \ll 1$, electron dynamics transverse to the propagation axis are non-relativistic. As we approach $a_0 \gtrsim 1$ transverse electron motion becomes relativistic within a single oscillation. We will neglect the change in momentum from emitting radiation when calculating the electron trajectory, known as radiation reaction. Quantum effects such as non-linear Compton scattering and electron-positron pair production are important when the fields become an appreciable fraction of the Schwinger limit in the electron rest frame; $E_{cr} = m_e^2 c^3/e\hbar \approx 1.3 \times 10^{16}$ V/cm and $B_{cr} = m_e^2 c^2/e\hbar \approx 4.4 \times 10^9$ T [Di +12]; throughout this thesis we restrict ourselves to the regime of classical electrodynamics, where fields in the electron's rest frame remain well below this limit.

The purpose of this thesis is to find conditions under which coherent photons in the $10 - 100$ keV

range can be obtained from the collision of counter propagating, relativistic electron bunches with a weak laser pulse $a_0 \ll 1$. In this case we expect reflected radiation around the Doppler shifted frequency $\omega \approx 4\gamma^2 \omega_0$ where γ is the initial Lorentz factor [Ein05]. Schemes of this nature have also been proposed by more recent authors such as Bulanov [Bul+13; BET03], who suggest this method could produce attosecond X-ray pulses, depending on the electron dynamics. One could generate a relativistic electron pulse using a linear accelerator, or a compact laser driven plasma based accelerator [ESL09]. For this investigation we will design and test a numerical code, capable of predicting the energy spectrum produced from a particular electron distribution interacting with an external electromagnetic field. In this thesis we use S.I. unit conventions, and we set $\hbar = c = \varepsilon_0 = 1$ to obtain natural units, unless explicitly stated otherwise. For a list of notation and conventions see Appendix A. The energy radiated per unit solid angle, per unit frequency by an arbitrary number of electrons each denoted by j, can be expressed as [Jac98, pg. 675, eqn. 14.65]

$$\frac{d^2 E}{d\omega d\Omega} = \frac{e^2}{16\pi^3} \left| \sum_j \int_{-\infty}^{\infty} \frac{\hat{\boldsymbol{n}} \times \left[(\hat{\boldsymbol{n}} - \boldsymbol{\beta}_j(t)) \times \dot{\boldsymbol{\beta}}_j(t) \right]}{(1 - \hat{\boldsymbol{n}} \cdot \boldsymbol{\beta}_j(t))^2} e^{i\omega[t - \hat{\boldsymbol{n}} \cdot \boldsymbol{r}_j(t)]} dt \right|^2 . \tag{1.1}$$

The spectrum of energy emitted can be determined providing we know each electron's trajectory $\boldsymbol{r}_j(t)$ and velocity $\boldsymbol{\beta}_j(t)$, for an observer in the direction of the dimensionless unit vector $\hat{\boldsymbol{n}}$ who measures radiation of frequency ω. One can derive equation (1.1) by solving Maxwell's equations with a point like charge and current to obtain the Liénard-Wiechert potentials and their corresponding fields; this is equivalent to solving Maxwell's equations with the Green's function method. These fields consist of a static term which varies with R^{-2}, and a term which depends on acceleration and varies with R^{-1}, where R is the distance of the observer from the electron at the time of emission (known as the retarded time) [Jac98, eqs. 14.13, 14.14]. For observers at large distances R, far away from the spatial extent of the electrons' trajectories, we retain only the second term and hence the unit vector pointing to the observer $\hat{\boldsymbol{n}}$, is approximately constant in time and for every electron. At this point Jackson proceeds to derive equation (1.1) by considering the Poynting vector from the Liénard - Wiechert fields, integrating over time to find energy, and then performing a Fourier decomposition to obtain the spectrum. This integral is performed in the observer's frame of reference who measures frequency ω, and the integration variable t is the retarded time. Note that the final polarisation of light is not measured. Equation (1.1) can be integrated by parts using the following derivative (1.2) [Jac98, eq. 14.66],

$$\frac{\hat{\boldsymbol{n}} \times \left[(\hat{\boldsymbol{n}} - \boldsymbol{\beta}_j(t)) \times \dot{\boldsymbol{\beta}}_j(t) \right]}{(1 - \hat{\boldsymbol{n}} \cdot \boldsymbol{\beta}_j(t))^2} = \frac{d}{dt} \left[\frac{\hat{\boldsymbol{n}} \times (\hat{\boldsymbol{n}} \times \boldsymbol{\beta}(t))}{1 - \hat{\boldsymbol{n}} \cdot \boldsymbol{\beta}_j(t)} \right], \tag{1.2}$$

$$\frac{d^2 E}{d\omega d\Omega} = \frac{e^2 \omega^2}{16\pi^3} \left| \sum_j \int_{-\infty}^{\infty} \hat{\boldsymbol{n}} \times (\hat{\boldsymbol{n}} \times \boldsymbol{\beta}_j(t)) \ e^{i\omega[t - \hat{\boldsymbol{n}} \cdot \boldsymbol{r}_j(t)]} dt \right|^2 . \tag{1.3}$$

The boundary terms have been discarded by assuming the motion is periodic, and that we are integrating over some integer multiple of the period T. We restrict our observation to harmonics $\omega = 2\pi l/T$ where l is an integer, and at this point the boundary terms vanish. Then by taking the limit $T \to \infty$ we recover a continuous spectrum of frequencies. Jackson instead proves equation (1.3) is equivalent to (1.1) by inserting a convergence factor $e^{-\epsilon|t|}$ for $\epsilon > 0$ in the integrand of

7

equation (1.1), and after integrating he takes the limit $\epsilon \to 0$ [Jac98]. Equation (1.1) shows that the energy radiated is identically zero during periods of no acceleration; this is not explicit for equation (1.3). This behavior is expected from the well known Larmor result, which describes the power radiated as proportional to the square of the acceleration, for one particle [Jac98, eq. 14.23]. We will refer to equations (1.1) and (1.3) interchangeably as 'radiation integrals'. In practice we will design our code to numerically integrate (1.1), but when solving for analytic solutions equation (1.3) is usually a simpler starting point. Numerically integrating integrals such as equation (1.3) has been attempted before, usually inside a particle-in-cell code (PIC) [RK10]. This is prohibitively slow for the small time steps needed to resolve high frequencies reflected from relativistic particles, according to the Nyquist theorem.

Earlier we cited laser wake field acceleration as a possible method for generating relativistic electrons [ESL09], this technique has the ability to produce high current, spin polarised bunches [WTK19]. Polarised beams of electrons allow for probing of fundamental, spin dependent processes in atomic, nuclear and particle physics [WTK19; Tol56], including symmetry breaking processes [Sch+13]. As we intend to numerically integrate electron trajectories to calculate the energy radiated, this information can also be used to model spin precession. One can show that the spin vector s in the rest frame of an electron precesses according to the Bargmann-Michel-Telegdi (BMT) equation [BPL82, § 41][BMT59]. We will adopt a form of the BMT equation used by Wen, Tamburini and Keitel [WTK19]:

$$\frac{d\boldsymbol{s}}{dt} = \boldsymbol{\Omega}(t, \boldsymbol{r}(t), \boldsymbol{\beta}(t)) \times \boldsymbol{s}, \tag{1.4}$$

$$\boldsymbol{\Omega}(t, \boldsymbol{r}(t), \boldsymbol{\beta}(t)) = \frac{e}{m_e} \left[\left(a_e + \frac{1}{\gamma(t)} \right) \boldsymbol{B}(t, \boldsymbol{r}(t)) - \left(a_e + \frac{1}{\gamma(t)+1} \right) \boldsymbol{\beta}(t) \times \boldsymbol{E}(t, \boldsymbol{r}(t)) \right.$$
$$\left. - \frac{a_e \gamma(t)}{\gamma(t)+1} \Big(\boldsymbol{\beta}(t) \cdot \boldsymbol{B}(t, \boldsymbol{r}(t)) \Big) \boldsymbol{\beta}(t) \right].$$

Where $a_e \approx 1.16 \times 10^{-3}$ is the anomalous electron magnetic moment, which takes into account radiative corrections to one loop [PS95, § 6.3]. All fields are stated in the laboratory frame of reference. A common procedure for deriving the BMT equation, is to write down the Hamiltonian in non-relativistic Quantum Mechanics, in the presence of an external field. In the Heisenberg picture we can take the expectation of the spin operator, to obtain an equation of motion for some classical spin vector s. One can then construct a covariant generalisation of this equation. Finally the equation listed above (1.4), can be obtained by assuming electron motion is well described by the covariant Lorentz equation. A full discussion can be found in Landau and Lifshitz volume 4 [BPL82, § 41] or by Jackson [Jac98, § 11.11]. Clearly the position, velocity and spin depend on the electron under consideration, but we assume each electron's spin precesses independently of one another, so there is no need insert a subscript j. Note that by taking the scalar product of equation (1.4) with s demonstrates the spin vector magnitude is always conserved, throughout our thesis it will be normalised $|\boldsymbol{s}| = 1$.

Chapter 2

Numerical code

This chapter outlines the algorithms used to calculate the spectrum of energy emitted from an arbitrary number of electrons. To do this we need to numerically integrate the trajectory of each particle and its radiation integral (1.1). Difficulties arise because these integrals are often rapidly oscillating, and the Doppler factor $1 - \hat{\boldsymbol{n}} \cdot \boldsymbol{\beta}$ on the denominator of equation (1.1), produces a sharp peak when observing parallel to the velocity for an ultra relativistic particle [RK10]. Throughout this thesis, we will often be concerned with radiation reflected from relativistic particles at frequencies given by the Doppler shift $\omega \approx 4\gamma^2\omega_0$ relative to the incident frequency ω_0. Observing these frequencies requires small time steps according to the Nyquist theorem. This suggests that using a particle in cell (PIC) code will be extremely slow. Instead we have chosen to write our own code.

Our program is structured around a Python (3.7.4) class named 'Simulation' [Pyt19]. The user can write a simple Python script initiating an instance of this class with fundamental properties of the particles involved: charge, mass, initial position and momenta for all particles etc. External fields are defined as functions which are passed to the Simulation class. The numerical integrators for the trajectory and radiation integrals, are stored as methods of the Simulation class. We make frequent use of the Numpy [Har+20] and Scipy [Vir+20] software packages throughout.

2.1 Ballistic movement of electrons

A significant overhead of PIC codes at each time step, is the need to calculate charge and current densities on a spatial grid from the position and velocities of macroparticles, which are used to advance the electromagnetic fields in time according to Maxwell's equations. Our code avoids this by only considering physical scenarios in which the electron motion is determined by external fields; one such example is ballistic motion, which we demonstrate as follows. Consider the Lorentz transformation of the electromagnetic field [Jac98];

$$\boldsymbol{E}' = \gamma \left(\boldsymbol{E} + \boldsymbol{\beta} \times \boldsymbol{B} \right) - \frac{\gamma^2}{\gamma + 1}(\boldsymbol{\beta} \cdot \boldsymbol{E})\boldsymbol{\beta}, \tag{2.1a}$$

$$\boldsymbol{B}' = \gamma \left(\boldsymbol{B} - \boldsymbol{\beta} \times \boldsymbol{E} \right) - \frac{\gamma^2}{\gamma + 1}(\boldsymbol{\beta} \cdot \boldsymbol{B})\boldsymbol{\beta}. \tag{2.1b}$$

A prime will denote a quantity in the electrons' rest frame. If the electron beam in question is initially

coherent and propagating through vacuum, we can expect the magnetic field in their common rest frame to be zero, $\boldsymbol{B}' = 0$. Then the laboratory magnetic field is linked to the electric field by a simple relation [Jac98];

$$\boldsymbol{B} = \boldsymbol{\beta} \times \boldsymbol{E}. \tag{2.2}$$

From this we can find the Lorentz force in the lab frame,

$$\boldsymbol{F}_L = -e \left(\frac{\boldsymbol{E}}{\gamma^2} - (\boldsymbol{\beta} \cdot \boldsymbol{E})\boldsymbol{\beta} \right). \tag{2.3}$$

Normally one would now argue for low density, relativistic electrons the inter-electron force transverse to the boost direction is heavily suppressed by the Lorentz factor squared [Sam+20]. If this is unsatisfactory, we can be explicit by calculating the Coulomb repulsion between two electrons in the rest frame and transform to the lab frame by inverting equation (2.1a),

$$\boldsymbol{E} = -\frac{\gamma e}{4\pi [d']^2} \left(\hat{\boldsymbol{r}} - \frac{\gamma}{\gamma + 1}(\boldsymbol{\beta} \cdot \hat{\boldsymbol{r}})\boldsymbol{\beta} \right). \tag{2.4}$$

Where $\hat{\boldsymbol{r}}$ is a dimensionless unit vector pointing from one electron to another and d' is their separation distance in the rest frame (which electron we consider is irrelevant here). Consider a laser of amplitude $a_0 = 0.02$ and optical wavelength $\lambda_0 = 0.8$ μm in the lab frame. This corresponds to an electric field of amplitude $E_0 = 2\pi m_e c^2 a_0 / e\lambda_0 \approx 8 \times 10^{10}$ V/m. Assume we have weakly relativistic electrons with Lorentz factor $\gamma = 10$ or energy 5.11 MeV and a separation in the order of one wavelength in the rest frame $d' \sim \lambda_0/\gamma$, given by a Lorentz contraction. With these parameters the term in front of the brackets in equation (2.4) can be used to estimate the electric field magnitude, which is in the order of $\sim 10^6$ V/m. Considering only the electric field, we can estimate the work done on an electron over one wavelength in the lab frame as ~ 1 eV, treating the electric field as constant and at its maximum initial value. This is so small, that no reasonable number of ballistically moving electrons at this density will produce enough repulsion to disperse in the lab frame over the time/length scales we are interested in; clearly such a beam can propagate ballistically before colliding with a laser pulse.

2.2   Runge-Kutta integrator for Lorentz equation

Restricting ourselves to low density electrons, initially moving ballistically before a collision with a weak laser pulse, the equations of motion for each electron can be determined entirely by the Lorentz equation for an external field:

$$\frac{d\boldsymbol{u}}{dt} = \boldsymbol{f}\left(t, \boldsymbol{r}(t), \boldsymbol{u}(t)\right), \tag{2.5}$$

$$\frac{d\boldsymbol{r}}{dt} = \frac{\boldsymbol{u}(t)}{\gamma(t)}, \tag{2.6}$$

$$\boldsymbol{f}\left(t, \boldsymbol{r}(t), \boldsymbol{u}(t)\right) = -\frac{e}{m_e} \left[\boldsymbol{E}(t, \boldsymbol{r}(t)) + \frac{\boldsymbol{u}(t)}{\gamma(t)} \times \boldsymbol{B}(t, \boldsymbol{r}(t)) \right], \tag{2.7}$$

$$\gamma(\boldsymbol{u}[t]) = \sqrt{1 + [\boldsymbol{u}(t)]^2}. \tag{2.8}$$

No reference to a specific electron j will be given in this section, as our discussion will be applied to every electron in the system independently. Our code always uses the dimensionless momentum $\boldsymbol{u} = \gamma\boldsymbol{\beta}$ (A.2), as opposed to the velocity which is restricted by the speed of light $|\boldsymbol{\beta}| < 1$. Therefore the momentum is less susceptible to numerical roundoff. Evaluating the radiation integral (1.1) is most convenient when the position and momentum are defined simultaneously. To this end we use a modified 4th order Runge-Kutta scheme (RK4). Numerical integration with the RK4 algorithm is covered by many mathematics [RHB06, § 27.6.4] and programming textbooks [Pre+92, § 16.1, § 16.2]. We note that the RK4 method is not symplectic, that is it does not conserve the volume of phase space and therefore the on shell condition $E^2 = m_e^2 \boldsymbol{u}^2 + m_e^2$ is not identically preserved.

We begin with the position $\boldsymbol{r}^m$ and momentum $\boldsymbol{u}^m$ at time t^m, and we wish to find the position $\boldsymbol{r}^{m+1}$ and momentum $\boldsymbol{u}^{m+1}$ at the next time step $t^{m+1} = t^m + \Delta t$. The initial quantities allow us to immediately estimate the change of momentum between time steps $\boldsymbol{k}_1$, using the Euler method. Now our approach differs from the usual explicit RK4 scheme as the electromagnetic fields (or $\boldsymbol{f}$ (2.7)) depend on the position. We get around this by using the change in momentum $\boldsymbol{k}_1$ from the previous step of the algorithm to estimate the position $\boldsymbol{r}^{m+1/2}$ needed to calculate $\boldsymbol{k}_2$. This can be achieved by discretising equation (2.6) with a leapfrog scheme

$$\frac{\boldsymbol{r}^{m+1/2} - \boldsymbol{r}^m}{\Delta t/2} = \frac{\boldsymbol{u}^{m+1/4}}{\gamma(\boldsymbol{u}^{m+1/4})} + O\left([\Delta t/2]^2\right), \tag{2.9}$$

and estimating the velocity at $m + 1/4$ using the change in momentum $\boldsymbol{k}_1$ which has already been calculated;

$$\boldsymbol{r}^{m+1/2} = \boldsymbol{r}^m + \frac{\Delta t}{2} \frac{\boldsymbol{u}^m + \boldsymbol{k}_1/4}{\gamma(\boldsymbol{u}^m + \boldsymbol{k}_1/4)} + O\left([\Delta t/2]^2\right). \tag{2.10}$$

If we repeat this procedure for each step of the RK4 algorithm, the full scheme becomes;

$$\boldsymbol{k}_1 = \Delta t\, \boldsymbol{f}\left(t^m, \quad \boldsymbol{r}^m, \quad \boldsymbol{u}^m\right), \tag{2.11a}$$

$$\boldsymbol{k}_2 = \Delta t\, \boldsymbol{f}\left(t^m + \frac{\Delta t}{2}, \quad \boldsymbol{r}^m + \frac{\Delta t}{2}\frac{\boldsymbol{u}^m + \boldsymbol{k}_1/4}{\gamma(\boldsymbol{u}^m + \boldsymbol{k}_1/4)}, \quad \boldsymbol{u}^m + \frac{\boldsymbol{k}_1}{2}\right), \tag{2.11b}$$

$$\boldsymbol{k}_3 = \Delta t\, \boldsymbol{f}\left(t^m + \frac{\Delta t}{2}, \quad \boldsymbol{r}^m + \frac{\Delta t}{2}\frac{\boldsymbol{u}^m + \boldsymbol{k}_2/4}{\gamma(\boldsymbol{u}^m + \boldsymbol{k}_2/4)}, \quad \boldsymbol{u}^m + \frac{\boldsymbol{k}_2}{2}\right), \tag{2.11c}$$

$$\boldsymbol{k}_4 = \Delta t\, \boldsymbol{f}\left(t^m + \Delta t, \quad \boldsymbol{r}^m + \Delta t\frac{\boldsymbol{u}^m + \boldsymbol{k}_3/2}{\gamma(\boldsymbol{u}^m + \boldsymbol{k}_3/2)}, \quad \boldsymbol{u}^m + \boldsymbol{k}_3\right). \tag{2.11d}$$

Now the momentum at the next time step is determined with the following weighted average

$$\boldsymbol{u}^{m+1} = \boldsymbol{u}^m + \frac{1}{6}\left(\boldsymbol{k}_1 + 2\boldsymbol{k}_2 + 2\boldsymbol{k}_3 + \boldsymbol{k}_4\right) + O\left([\Delta t]^5\right). \tag{2.12}$$

Here we have stated the local error of order $O\left([\Delta t]^5\right)$ for a single step, which would accumulate to a global error of $O\left([\Delta t]^4\right)$ in a usual RK4 scheme. In practice, our hybrid scheme will introduce

an additional error from estimating the position to second order at each step to evaluate the fields. This additional error depends on the variation of the fields with position. In the interest of avoiding any further function calls, we can determine the position to second order using our leapfrog scheme again. The velocity at the midpoint is estimated by averaging between time steps.

$$\boldsymbol{r}^{m+1} = \boldsymbol{r}^m + \Delta t\, \boldsymbol{u}^{m+1/2} = \boldsymbol{r}^m + \frac{\Delta t}{2}\left(\frac{\boldsymbol{u}^m}{\gamma(\boldsymbol{u}^m)} + \frac{\boldsymbol{u}^{m+1}}{\gamma(\boldsymbol{u}^{m+1})}\right) + O\left([\Delta t]^2\right). \qquad (2.13)$$

This procedure is repeated until the complete trajectories and momenta of all particles in the system are found, for some time interval. In practice, due to the small time step needed to resolve high frequencies in the spectra (2.16), numerically integrating the trajectory for many particles is the most intensive task our program must perform. There are a couple of ways we have sped up our code; by pre-compiling regularly used functions such as the Lorentz equation (2.7) using the 'just-in-time' methods provided by Numba [LPS15]. We frequently use a cluster when running these scripts with many particles, and as each particle's trajectory is integrated independently from one another we can easily split the workload over several nodes using the Message Passing Interface for Python (MPI4PY) [Dal+11]. Note that this numerical integrator could easily be extended to take into account radiative losses when calculating the trajectory, simply by replacing $\boldsymbol{f}$ in equation (2.7) with the Landau-Lifshitz equation [Pia08].

2.3   Fast Fourier transform method for radiation integral

Before proceeding we first need to rewrite the radiation integral (1.1) in terms of the dimensionless momentum our numerical code uses. This is easily done by differentiating the definition $\boldsymbol{u}(t) = \gamma(t)\boldsymbol{\beta}(t)$ with respect to time (as indicated by a dot), and using the derivative of the Lorentz factor

$$\dot{\gamma}(t) = \frac{\boldsymbol{u}\cdot\dot{\boldsymbol{u}}}{\gamma}, \qquad (2.14)$$

to obtain a relation between both acceleration-like quantities $\dot{\boldsymbol{\beta}}$ and $\dot{\boldsymbol{u}}$,

$$\dot{\boldsymbol{\beta}} = \frac{\dot{\boldsymbol{u}}}{\gamma} - (\boldsymbol{u}\cdot\dot{\boldsymbol{u}})\,\frac{\boldsymbol{u}}{\gamma^3}. \qquad (2.15)$$

Substituting the acceleration $\dot{\boldsymbol{\beta}}$ (2.15) into the radiation integral (1.1) for each particle denoted by j, we obtain

$$\frac{d^2E}{d\omega d\Omega} = \frac{e^2}{16\pi^3}\left|\sum_j \int_{t_i}^{t_f} \frac{\hat{\boldsymbol{n}}\times\left(\hat{\boldsymbol{n}}\times\left[\gamma_j^2\dot{\boldsymbol{u}}_j - (\boldsymbol{u}_j\cdot\dot{\boldsymbol{u}}_j)\boldsymbol{u}_j\right] - \gamma_j\boldsymbol{u}_j\times\dot{\boldsymbol{u}}_j\right)}{\gamma_j(\gamma_j - \hat{\boldsymbol{n}}\cdot\boldsymbol{u}_j)^2}\, e^{i\omega[t-\hat{\boldsymbol{n}}\cdot\boldsymbol{r}_j]}dt\right|^2. \qquad (2.16)$$

Where the time dependence of the position $\boldsymbol{r}_j$, momentum $\boldsymbol{u}_j$ and the Lorentz factor γ_j is implied. In practice, we always define the initial values for every particle simultaneously at t_i, and the final time t_f is chosen when all particles are no longer interacting with the external fields. If an

electron has non-zero acceleration at t_i this suggests we are neglecting radiation emitted before the simulation begins, and subsequent interference. This suggests t_i should be chosen when all particles have zero acceleration.

The radiation integral (2.16) must now be numerically evaluated. We start by approximating the integral inside the square modulus as a Riemann sum for each particle,

$$\boldsymbol{K}_j(\omega) = \Delta t \sum_{m=0}^{N_t-1} \boldsymbol{\mathcal{F}}_j[m] \, e^{i\omega \mathcal{T}_j[m]}. \tag{2.17}$$

Where the integral has been broken into N_t equally spaced time steps, $\Delta t = (t_f - t_i)/N_t$. The integrand is now determined by the j th particle's momenta and trajectory from the RK4 algorithm at the m th time step,

$$\boldsymbol{\mathcal{F}}_j[m] = \frac{\hat{\boldsymbol{n}} \times \left(\hat{\boldsymbol{n}} \times \left[(\gamma_j^m)^2 \dot{\boldsymbol{u}}_j^m - (\boldsymbol{u}_j^m \cdot \dot{\boldsymbol{u}}_j^m) \boldsymbol{u}_j^m \right] - \gamma_j^m \boldsymbol{u}_j^m \times \dot{\boldsymbol{u}}_j^m \right)}{\gamma_j^m (\gamma_j^m - \hat{\boldsymbol{n}} \cdot \boldsymbol{u}_j^m)^2}. \tag{2.18}$$

$$\mathcal{T}_j[m] = t_i + m\Delta t - \boldsymbol{n} \cdot \boldsymbol{r}_j^m \tag{2.19}$$

The Lorentz factor has been determined at each time step according to $\gamma_j^m = \sqrt{1 + (\boldsymbol{u}_j^m)^2}$. Approximating the radiation integral as a Riemann sum is only possible because $\mathcal{T}_j$ is monotonically increasing with time; if we take the derivative before discretisation in equation (2.19) we see $d\mathcal{T}_j/dt = 1 - \hat{\boldsymbol{n}} \cdot \boldsymbol{\beta} > 0$ because the electron can never propagate faster than the speed of light. There are several different approaches one could take to calculate $\boldsymbol{K}_j$ (2.17). We could directly evaluate each term and add. This would be very computationally expensive $O(N_t^{d+1})$; where O refers to the run time or resource requirements in computer science, and d is the dimension of the Fourier Transform, in this case $d = 3$. Instead we will treat equation (2.17) as a discrete Fourier transform in the dummy variable $\mathcal{T}_j$. While our data was equally spaced in time it will not in general be equally spaced in $\mathcal{T}_j$, so we cannot use a common FFT algorithm like Cooley-Tukey [CT65]. Instead we use a non-equispaced fast Fourier transform (NFFT) developed by Keiner, Kunis and Potts [KKP09, NFFT3]. Their algorithm interpolates between unequally spaced data points using a window function, to approximate an equally spaced data set which can be used with a FFT. These algorithms are provided as a C library, so we have also used a Python wrapper developed by Vanderplas to implement this in our code [Van17].

Overall, our program calculates the momenta and trajectories of each particle using the RK4 method, from which $\boldsymbol{\mathcal{F}}_j$ and $\mathcal{T}_j$ are calculated. These quantities are passed to the NFFT3 algorithm, which calculates $\boldsymbol{K}_j$ at the following N_t discrete frequencies

$$\omega = \frac{2\pi f_s}{N_t} \left[0, 1, \ldots, \frac{N_t}{2} - 1 \right], \qquad \text{sample frequency: } f_s = \frac{1}{\Delta t}. \tag{2.20}$$

Where the maximum frequency is determined by the Nyquist theorem according to the step size. Taking the sum of $\boldsymbol{K}_j$ over all particles and the square modulus, determines the spectral energy radiated (2.21),

$$\frac{d^2E}{d\omega d\Omega} = \frac{e^2}{16\pi^3} \left| \sum_j \boldsymbol{K}_j[\omega] \right|^2.$$ (2.21)

2.4 Runge-Kutta integrator for Bargmann-Michel-Telegdi equation

At each time step of our simulation, we must advance the spin vector's rotation. Electron spin precession as determined by the BMT equation (1.4) can be rewritten in terms of momentum $\boldsymbol{u}$,

$$\frac{d\boldsymbol{s}}{dt} = \boldsymbol{g}\big(t, \boldsymbol{r}(t), \boldsymbol{u}(t), \boldsymbol{s}(t)\big),$$

$$\boldsymbol{g}\big(t, \boldsymbol{r}(t), \boldsymbol{u}(t), \boldsymbol{s}(t)\big) = \frac{e}{m_e} \left[\left(a_e + \frac{1}{\gamma(t)} \right) \boldsymbol{B}(t, \boldsymbol{r}(t)) - \left(a_e + \frac{1}{\gamma(t) + 1} \right) \frac{\boldsymbol{u}(t) \times \boldsymbol{E}(t, \boldsymbol{r}(t))}{\gamma(t)} \right.$$

$$\left. - \frac{a_e}{\gamma(t) + 1} \left(\frac{\boldsymbol{u}(t) \cdot \boldsymbol{B}(t, \boldsymbol{r}(t))}{\gamma(t)} \right) \boldsymbol{u}(t) \right] \times \boldsymbol{s}(t).$$ (2.22)

Applying the same method used to obtain the momentum and position, we discretise both of these equations and use the RK4 algorithm. Spin $\boldsymbol{s}^m$ is known at time t^m, and we wish to find $\boldsymbol{s}^{m+1}$ at time $t^{m+1} = t^m + \Delta t$. By inserting the same momentum and position estimates at each RK4 step from our calculation of the trajectory (2.11),

$$\boldsymbol{l}_1 = \Delta t \, \boldsymbol{g}\Big(t^m, \quad \boldsymbol{r}^m, \quad \boldsymbol{u}^m, \quad \boldsymbol{s}^m\Big),$$ (2.23a)

$$\boldsymbol{l}_2 = \Delta t \, \boldsymbol{g}\left(t^m + \frac{\Delta t}{2}, \quad \boldsymbol{r}^m + \frac{\Delta t}{2} \frac{\boldsymbol{u}^m + \boldsymbol{k}_1/4}{\gamma(\boldsymbol{u}^m + \boldsymbol{k}_1/4)}, \quad \boldsymbol{u}^m + \frac{\boldsymbol{k}_1}{2}, \quad \boldsymbol{s}^m + \frac{\boldsymbol{l}_1}{2}\right),$$ (2.23b)

$$\boldsymbol{l}_3 = \Delta t \, \boldsymbol{g}\left(t^m + \frac{\Delta t}{2}, \quad \boldsymbol{r}^m + \frac{\Delta t}{2} \frac{\boldsymbol{u}^m + \boldsymbol{k}_2/4}{\gamma(\boldsymbol{u}^m + \boldsymbol{k}_2/4)}, \quad \boldsymbol{u}^m + \frac{\boldsymbol{k}_2}{2}, \quad \boldsymbol{s}^m + \frac{\boldsymbol{l}_2}{2}\right),$$ (2.23c)

$$\boldsymbol{l}_4 = \Delta t \, \boldsymbol{g}\left(t^m + \Delta t, \quad \boldsymbol{r}^m + \Delta t \frac{\boldsymbol{u}^m + \boldsymbol{k}_3/2}{\gamma(\boldsymbol{u}^m + \boldsymbol{k}_3/2)}, \quad \boldsymbol{u}^m + \boldsymbol{k}_3, \quad \boldsymbol{s}^m + \boldsymbol{l}_3\right).$$ (2.23d)

This is computationally inexpensive as no additional function calls to the fields are necessary, every quantity needed aside from the spin estimates has already been calculated for the trajectory (2.11). As with the momentum (2.12), we can perform a weighted sum of the derivatives to calculate the new spin,

$$\boldsymbol{s}^{m+1} = \boldsymbol{s}^m + \frac{1}{6} \left(\boldsymbol{l}_1 + 2\boldsymbol{l}_2 + 2\boldsymbol{l}_3 + \boldsymbol{l}_4 \right) + O\left([\Delta t]^5\right).$$ (2.24)

Once again we have stated the local error for one time step as $O\left([\Delta t]^5\right)$ which excludes any additional error from the estimation of position, at each step of the RK4 algorithm.

Chapter 3

Constant magnetic field

Having written a numerical code, we should test it against an exact analytic solution to demonstrate its accuracy. One such benchmark is the helical motion of electrons in a constant magnetic field. This problem has been studied extensively before. The earliest derivation we can find of the spectral energy radiated by an electron in circular motion is by Schwinger [Sch49, section III]. Jackson extends this to several electrons evenly distributed around a circle executing the same periodic motion [Jac98, problems 14.15, 14.23], which is the specific problem we are interested in. The goal of our derivation is to reproduce these results while also proving that only harmonics of the cyclotron frequency are emitted, this is simply assumed by the derivations of Jackson and Schwinger. Finally we reference a derivation by Salamin and Faisal [SF96, Appendix A], who consider single electron motion in a circularly polarised plane wave; we use a similar method to obtain the power radiated per unit solid angle into the m th harmonic. To provide physical justification, this scenario can be considered similar to electrons moving in a closed circuit with a constant drift velocity in a conductor.

3.1 Equations of Motion

We start from the Lorentz equation with a constant magnetic field of magnitude B_0 along the $\hat{\boldsymbol{y}}$ axis,

$$m_e \frac{d(\gamma \boldsymbol{\beta}(t))}{dt} = -e\boldsymbol{\beta}(t) \times B_0 \hat{\boldsymbol{y}}. \tag{3.1}$$

Taking the scalar product of equation (3.1) with the velocity $\boldsymbol{\beta}$ demonstrates that $\boldsymbol{\beta}^2$ and therefore the Lorentz factor γ are conserved. For an electron with initial velocity $\beta_0 \hat{\boldsymbol{x}}$ at the origin the equations of motion can be written:

$$\boldsymbol{\beta}(t) = \beta_0 \begin{pmatrix} \cos(\omega_c t) \\ 0 \\ -\sin(\omega_c t) \end{pmatrix}, \qquad \boldsymbol{r}(t) = \frac{\beta_0}{\omega_c} \begin{pmatrix} \sin(\omega_c t) \\ 0 \\ \cos(\omega_c t) - 1 \end{pmatrix}. \tag{3.2}$$

Where $\omega_c = eB_0/m_e\gamma$ is the cyclotron frequency and $T = 2\pi/\omega_c$ is the period of oscillation. This is the usual circular motion of an electron in a plane perpendicular to a magnetic field. The magnetic

field should be 'switched on' for the interval $-NT \leqslant t \leqslant NT$ and zero at all other times, so the electrons do not accelerate or radiate energy before the simulation begins. It is our intention to use these equations of motion to solve the radiation integral given by equation (1.3). We start by defining our observation direction $\hat{\boldsymbol{n}} = (\cos(\phi), \sin(\phi), 0)$ with one component parallel and one perpendicular to the plane of motion. Using this we can derive some algebraic results;

$$\hat{\boldsymbol{n}} \cdot \boldsymbol{r}(t) = \frac{\beta_0}{\omega_c} \cos(\phi) \sin(\omega_c t), \tag{3.3}$$

$$\hat{\boldsymbol{n}} \times (\hat{\boldsymbol{n}} \times \boldsymbol{\beta}(t)) = \beta_0 \sin(\phi) \cos(\omega_c t) \left[-\sin(\phi)\hat{\boldsymbol{x}} + \cos(\phi)\hat{\boldsymbol{y}} \right] + \beta_0 \sin(\omega_c t)\hat{\boldsymbol{z}},$$

$$\Rightarrow \beta_0 \sin(\phi) \cos(\omega_c t)\hat{\boldsymbol{z}} \times \hat{\boldsymbol{n}} + \beta_0 \sin(\omega_c t)\hat{\boldsymbol{z}}. \tag{3.4}$$

We can now write down the radiation integral (1.3) for N_p particles

$$\frac{d^2 E}{d\omega d\Omega} = \frac{e^2 \omega^2}{16\pi^3} \left| \sum_{j=0}^{N_p-1} \boldsymbol{K}_j \right|^2. \tag{3.5}$$

3.2   Solution of the radiation integral

The particle with equations of motion (3.2) will be referred to as the zeroth particle $j = 0$, and will have an associated integral $\boldsymbol{K}_0$. Using the algebraic results above, equations (3.3) and (3.4), to calculate the integrand our radiation integral (1.3) can be written for this particle as,

$$\boldsymbol{K}_0 = \int_{-NT}^{NT} \beta_0 \left[\sin(\phi) \cos(\omega_c t)\hat{\boldsymbol{z}} \times \hat{\boldsymbol{n}} + \sin(\omega_c t)\hat{\boldsymbol{z}} \right] \; e^{i\frac{\omega}{\omega_c}[\omega_c t - \beta_0 \cos(\phi) \sin(\omega_c t)]} dt \tag{3.6}$$

Consider an ensemble of electrons equally distributed around a circle, undergoing the same periodic motion. The equations of motion and integral for each particle are identical to those for $j = 0$ apart from a constant phase shift. Or equivalently, we can consider the orbit of particle j to be identical to $j = 0$ if it started at a later time obtained from the substitution $t \to t + jT/N_p$, which allows us to write the integral for a general particle,

$$\boldsymbol{K}_j = \int_{-NT+\frac{jT}{N_p}}^{NT+\frac{jT}{N_p}} \beta_0 \left[\sin(\phi) \cos\left(\omega_c \left[t + \frac{jT}{N_p}\right]\right) \hat{\boldsymbol{z}} \times \hat{\boldsymbol{n}} + \sin\left(\omega_c \left[t + \frac{jT}{N_p}\right]\right) \hat{\boldsymbol{z}} \right]$$
$$e^{i\frac{\omega}{\omega_c}\left[\omega_c t - \beta_0 \cos(\phi) \sin\left(\omega_c \left[t + \frac{jT}{N_p}\right]\right)\right]} dt. \tag{3.7}$$

By a simple change of integration variable, we can see this is identical to our integral for $j = 0$ (3.6) apart from a constant phase term.

$$\boldsymbol{K}_j = e^{-i \, 2\pi\omega j/N_p\omega_c} \, \boldsymbol{K}_0. \tag{3.8}$$

Therefore we only need to solve the integral for $j = 0$ to obtain the total energy radiated from all particles,

$$\frac{d^2E}{d\omega d\Omega} = \frac{e^2\omega^2}{16\pi^3} \left| \sum_{j=0}^{N_p-1} F_j(\omega) \right|^2 \left| \mathbf{K}_0 \right|^2, \qquad \text{where } F_j(\omega) = e^{-i\, 2\pi\omega j/N_p\omega_c}. \tag{3.9}$$

The generating function for Bessel functions of the first kind [AS64, eq. 9.1.41],

$$e^{iz\sin(\theta)} = \sum_{m=-\infty}^{\infty} J_m(z)e^{im\theta}, \tag{3.10}$$

can be used to expand $\mathbf{K}_0$ (3.6) in an infinite series of Bessel functions. We will demonstrate this process greatly simplifies the resulting integral,

$$\mathbf{K}_0 = \beta_0 \int_{-NT}^{NT} \sum_{m=-\infty}^{\infty} [\sin(\phi)\cos(\omega_c t)\hat{\mathbf{z}} \times \hat{\mathbf{n}} + \sin(\omega_c t)\hat{\mathbf{z}}] \; J_m(x) \; e^{i(\omega - m\omega_c)t}dt, \qquad x = \frac{\omega}{\omega_c}\beta_0\cos(\phi). \tag{3.11}$$

To obtain equation (3.11) we have used the well known properties of Bessel functions for negative arguments and integer orders, $J_m(-x) = J_{-m}(x) = (-1)^m J_m(x)$. The integrand of equation (3.11) can be rewritten by replacing each sinusoidal function with a Bessel function, and using the recurrence relations of Bessel functions to simplify [AS64, pg. 361, eq. 9.1.27];

$$\sum_{m=-\infty}^{\infty} J_m(x)\cos(\omega_c t) \; e^{-im\omega_c t} = \frac{1}{2} \sum_{m=-\infty}^{\infty} J_m(x) \left(e^{-i(m-1)\omega_c t} + e^{-i(m+1)\omega_c t} \right),$$

$$\Rightarrow \frac{1}{2} \sum_{m=-\infty}^{\infty} [J_{m+1}(x) + J_{m-1}(x)] \; e^{-im\omega_c t} = \sum_{m=-\infty}^{\infty} \frac{m}{x} J_m(x) \; e^{-im\omega_c t}. \tag{3.12}$$

$$\sum_{m=-\infty}^{\infty} J_m(x)\sin(\omega_c t)e^{-im\omega_c t} = \frac{1}{2i} \sum_{m=-\infty}^{\infty} J_m(x) \left(e^{-i(m-1)\omega_c t} - e^{-i(m+1)\omega_c t} \right),$$

$$\Rightarrow \frac{1}{2i} \sum_{m=-\infty}^{\infty} [J_{m+1}(x) - J_{m-1}(x)] \; e^{-im\omega_c t} = i \sum_{m=-\infty}^{\infty} \frac{dJ_m}{dx} e^{-im\omega_c t}. \tag{3.13}$$

Using equations (3.12) and (3.13), and exchanging the order of summation and integration we can reduce $\mathbf{K}_0$ (3.11) to the following integral,

$$\mathbf{K}_0 = \beta_0 \sum_{m=-\infty}^{\infty} \left[\frac{m}{x}\sin(\phi)J_m(x)\hat{\mathbf{z}} \times \hat{\mathbf{n}} + i\frac{dJ_m}{dx}\hat{\mathbf{z}} \right] \int_{-NT}^{NT} e^{i(\omega - m\omega_c)t}dt. \tag{3.14}$$

The remaining integral is easy to solve, and we recognise its asymptotic behaviour as a Dirac delta when $N \to \infty$, we can see already that this will restrict emission to fixed harmonics of the cyclotron frequency.

17

$$\int_{-NT}^{NT} e^{i(\omega - m\omega_c)t} dt = \frac{2\sin([\omega - m\omega_c]NT)}{\omega - m\omega_c} \rightarrow 2\pi\delta(\omega - m\omega_c) \qquad \text{as } N \rightarrow \infty \qquad (3.15)$$

3.3 Average power per unit solid angle emitted into each harmonic

Recalling our integral is defined for $2N$ oscillations, we can write the total power radiated per unit solid angle averaged over one oscillation as

$$\frac{dP}{d\Omega} = \int_{-\infty}^{\infty} \lim_{N \to \infty} \frac{1}{2NT} \left(\frac{d^2E}{d\omega d\Omega} \right) d\omega. \qquad (3.16)$$

To solve (3.16) we must expand the square modulus $| \, \boldsymbol{K}_0 \, |^2$ (3.14). In general this is a double sum with a product of two integrals of the kind seen in (3.15). Applying the limit to one of the integrals will result in a delta function (3.15), which collapses the expression into a single sum. Keeping in mind the second integral is multiplied by this delta function, we can expand out the $\sin$ function for small arguments (3.15), cancelling out the factor of $2NT$ in (3.16). Integrating the remaining sum and delta function over frequency will restrict the emitted radiation to harmonics of the cyclotron frequency,

$$\frac{dP}{d\Omega} = \frac{e^2\beta_0^2}{8\pi^2} \sum_{m=-\infty}^{\infty} \left[m^2\omega_c^2 \left| \sum_{j=0}^{N_p-1} F_j(m\omega_c) \right|^2 \left(\left[\frac{dJ_m}{dx} \right]^2 + \frac{\tan^2(\phi)}{\beta_0^2} \left[J_m(x) \right]^2 \right) \right]. \qquad (3.17)$$

From this we can identify the power radiated into the m th harmonic,

$$\frac{dP_m}{d\Omega} = \frac{e^2\beta_0^2 m^2\omega_c^2}{8\pi^2} \left| \sum_{j=0}^{N_p-1} F_j[m] \right|^2 \left(\left[\frac{dJ_m}{dx} \right]^2 + \frac{\tan^2(\phi)}{\beta_0^2} \left[J_m(x) \right]^2 \right), \qquad (3.18)$$

$$\text{where} \qquad F_j[m] = e^{-i\,2\pi mj/N_p}, \qquad \text{and} \qquad x = m\beta_0\cos(\phi).$$

This derivation is our own work, designed to demonstrate only harmonics are emitted from periodic motion. However this result has been obtained before for a single electron by Schwinger [Sch49, eq. III.28], and for many electrons by Jackson [Jac98, problems 14.15, 14.23], who use a different method based on the Poisson sum formula.

3.4 Single electron: trajectory and spectrum of radiation emitted

Consider a single electron with the equations of motion listed above (3.2). Choosing a relatively small Lorentz factor $\gamma = 5$, confines emission to low multiples of the cyclotron frequency, so we can easily observe the harmonic behaviour. This is equivalent to choosing an initial momentum $u_{0x} = \sqrt{\gamma^2 - 1}$ in our numerical code, or velocity $\beta_0 = u_{0x}/\gamma$ in our analytic solutions (3.2). Our numerical code requires a magnitude for the magnetic field, so we choose $B_0 = 1\,T$; this choice is completely arbitrary, and in fact we have normalised all of our results relative to the cyclotron frequency ω_c

such that this choice is irrelevant to the plots produced. Initially this simulation is performed for one oscillation to produce the trajectory and average power radiated in Figure 3.1a, this leads to a resolution in frequency of exactly the cyclotron frequency according to the Nyquist theorem. As the motion is periodic we can instead average our numerical result over ten oscillations, seen in Figure 3.1b, to effectively increase the resolution and demonstrate only harmonics of the cyclotron frequency are emitted.

After computing the numerical results we turn our attention to the analytic solutions. To evaluate the Bessel functions in equation (3.18) to a high degree of accuracy, we can use the SciPy library for special functions [Vir+20].

Clearly the trajectory of the electron is correct, however the accuracy of the numerical solutions is somewhat meaningless because of the small time step that was needed to solve the spectrum. The power radiated per unit solid angle, as a function of the angle ϕ relative to the plane of orbit can be seen in Figure 3.1a and Figure 3.1b. Most of the energy, in particular at high frequencies tends to be radiated closer to the plane of orbit. Note that Figure 3.1a may be somewhat misleading; the continuous line implies that power is emitted at all frequencies. This is why Figure 3.1b has been included to prove only harmonic emission is allowed.

3.5   Spin precession of a single electron

When an electron moves with equations of motion (3.2), its spin precession will be independent from the momentum, no electric field is present and the $\boldsymbol{u} \cdot \boldsymbol{B}$ term is zero. The BMT equation in these circumstances is given by (1.4),

$$\frac{d\boldsymbol{s}}{dt} = \frac{e}{m_e} \left(a_e + \frac{1}{\gamma} \right) \boldsymbol{B} \times \boldsymbol{s}(t). \tag{3.19}$$

Where the magnetic field is constant, and the Lorentz factor conserved. This is equivalent to three differential equations,

$$\frac{ds_x}{dt} = \omega_c(a_e\gamma + 1) \, s_z(t), \tag{3.20a}$$

$$\frac{ds_y}{dt} = 0, \tag{3.20b}$$

$$\frac{ds_z}{dt} = -\omega_c(a_e\gamma + 1) \, s_x(t). \tag{3.20c}$$

Which have similar solutions to the Lorentz equation for a constant magnetic field:

$$s_x(t) = s_{0x} \cos(\omega_c[a_e\gamma + 1]t) + s_{0z} \sin(\omega_c[a_e\gamma + 1]t), \tag{3.21}$$

$$s_y(t) = s_{0y}, \tag{3.22}$$

$$s_z(t) = s_{0z} \cos(\omega_c[a_e\gamma + 1]t) - s_{0x} \sin(\omega_c[a_e\gamma + 1]t). \tag{3.23}$$
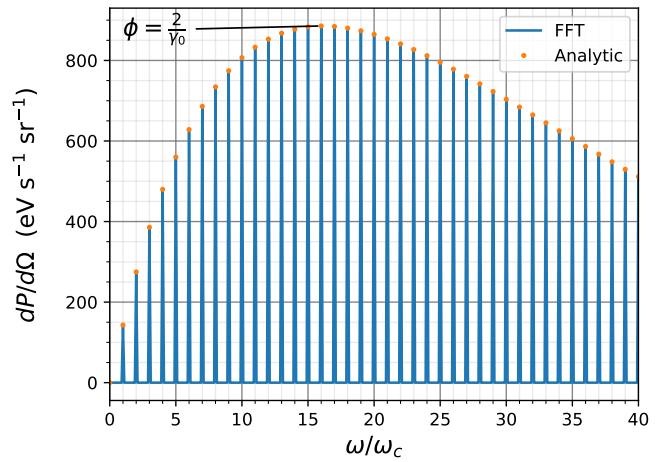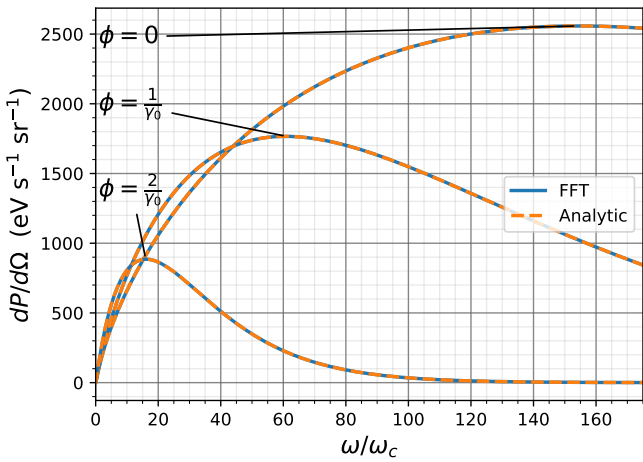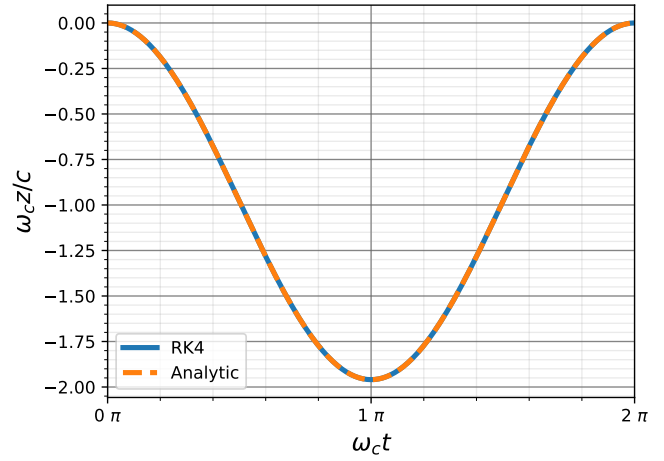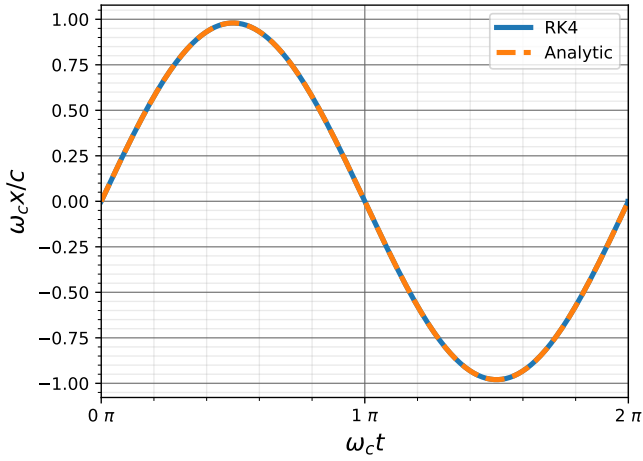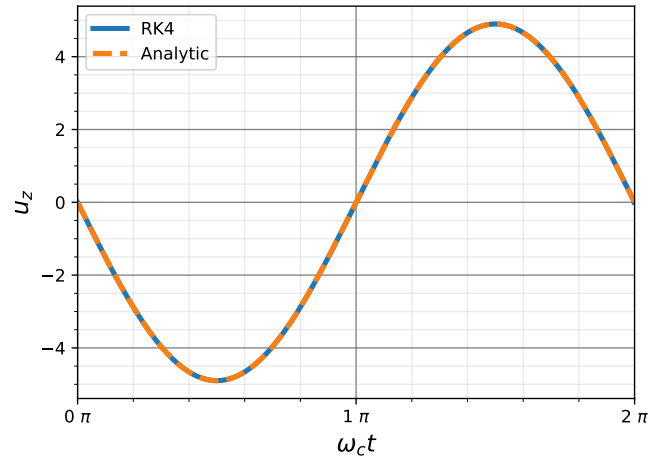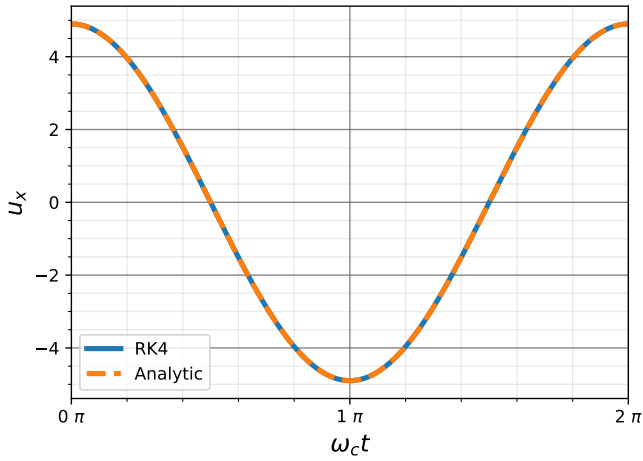
(a) Averaged over 1 oscillation

(b) Averaged over 10 oscillations

Figure 3.1: Trajectory and power emitted by a single electron in a constant magnetic field. Analytic solutions for momentum and position are given by equation (3.2). Plotting the power emitted, averaged over many time periods, achieves a higher resolution in frequency demonstrating only harmonics of the cyclotron frequency are emitted; analytic solutions are given by (3.18).

Ignoring the small contribution provided by the magnetic moment anomaly a_e, it is well known from the classical Larmor equation that spin precesses around a magnetic field with constant magnitude. The results of our simulation can be seen in Figure 3.2, where an initial spin of $s_x = s_z = 1/\sqrt{2}$ with no component parallel to the magnetic field $s_y = 0$, and a Lorentz factor $\gamma = 5$ has been selected to be consistent with the results in Figure 3.1. The BMT equation (3.19) predicts the spin vector will oscillate with frequency $\omega_s = \omega_c(a_e\gamma + 1)$. However the anomalous correction a_e is too small to be observed over one cycle, so it appears that the momentum and spin oscillate with the cyclotron frequency.
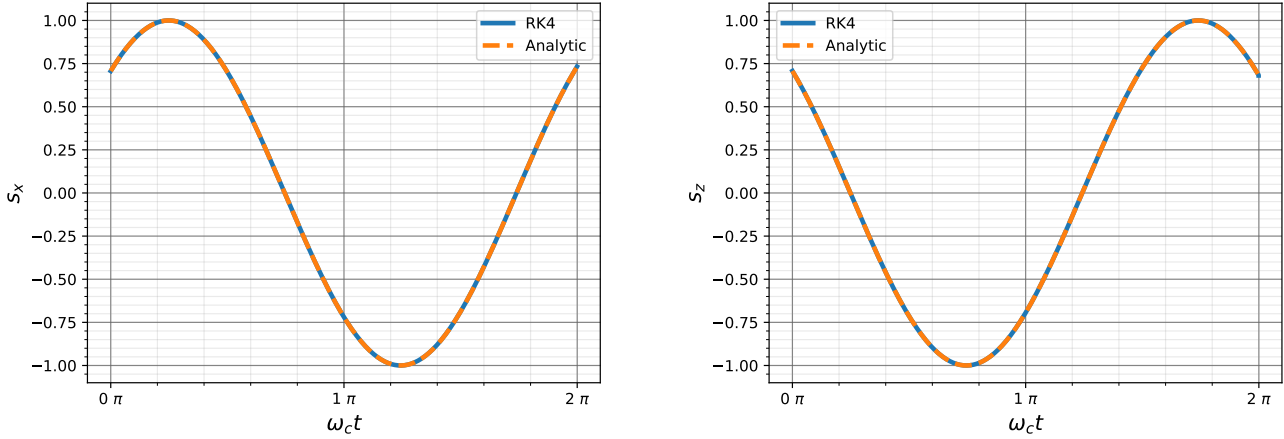
Figure 3.2: Spin precession in a constant magnetic field. Analytic solutions are provided by equations (3.21), (3.22) and (3.23). The spin vector is normalised to 1 at all times.

3.6 Coherence effects with multiple electrons

Having established that our numerical code works accurately for a single electron, we can extend our analysis to two electrons. Consider the scenario used to derive equation (3.18), several electrons equally distributed around a circle executing the same periodic motion. Each of our simulations average the power radiated over ten oscillations to reduce the effective time step, as seen earlier for one electron in Figure 3.1b, to discern the harmonics emitted. Much of the physics involved is apparent from the sum of oscillatory terms F present in equation (3.18). If the electrons radiate coherently, the average power emitted should be proportional to the number of electrons squared N_p^2.

Figure 3.3a shows the energy radiated for two electrons at every harmonic, emission only occurs for even harmonics, so we have plotted this against the one electron case in Figure 3.3b. One can see even harmonics have increased by a factor of $N_p^2 = 4$ for two electrons compared to one. By expanding out the sum of oscillatory terms in equation (3.18), we can easily show only even harmonics are permitted, $|1 + e^{-i\pi m}|^2 = |1 + (-1)^m|^2$.

As the number of electrons tends to infinity no radiation is emitted whatsoever, which can be seen by approximating the sum of constant phase terms (3.18) as an integral under the following limit;

$$\lim_{N_p \to \infty} \sum_{j=0}^{N_p-1} e^{-2\pi i\ mj/N_p} = \lim_{N_p \to \infty} (N_p) \int_0^1 e^{-2\pi i\ mx} dx = 0, \tag{3.24}$$

which is independent of the harmonic chosen. At this limit the charge distribution becomes continuous and is therefore analogous to a circuit of electrons, where the current becomes steady and the emitted magnetic field is static, and no radiation is emitted. However in a real conductor, static positive ions neutralise the charge density of negative electrons.
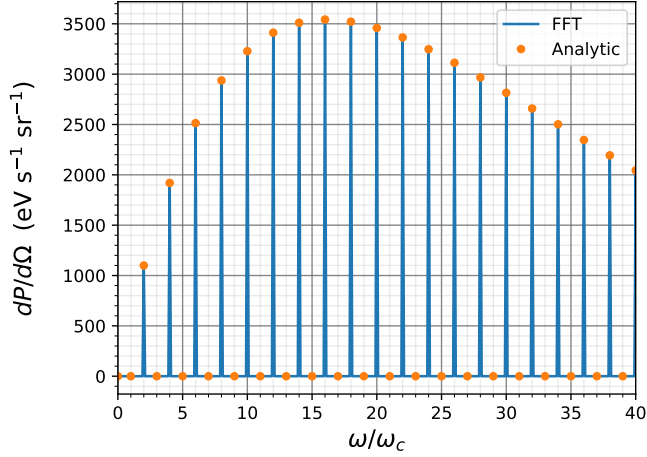
(a) $N_p = 2$
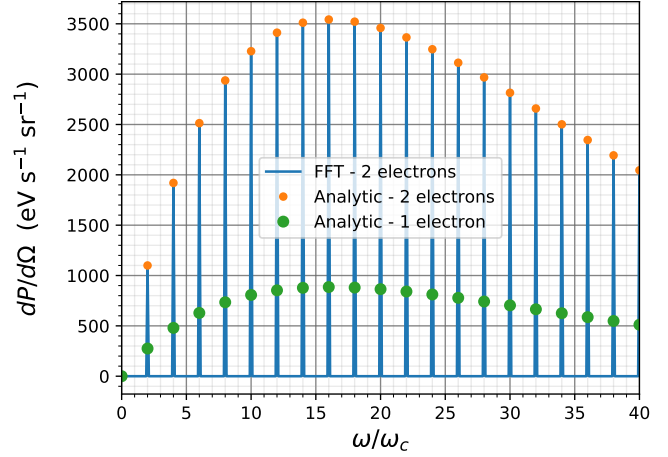
(b) Even harmonics only, $N_p = 1$ and $N_p = 2$
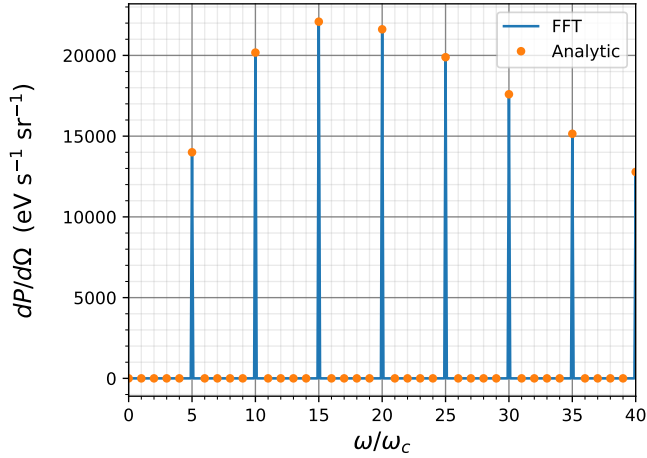
(c) $N_p = 5$
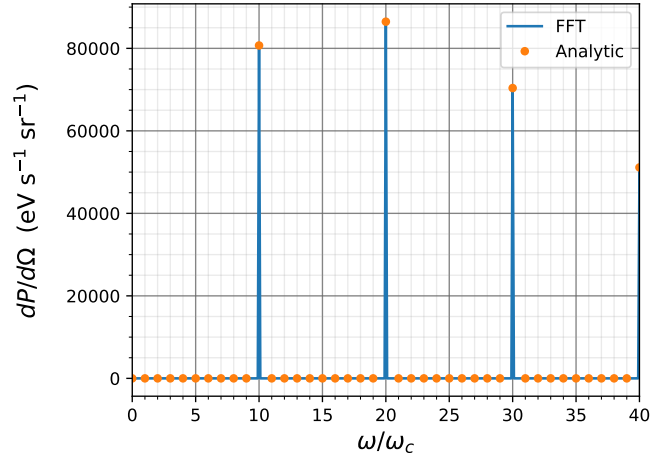
(d) $N_p = 10$

Figure 3.3: Spectra emitted from N_p electrons at angle $\phi = 2/\gamma_0$ in a constant magnetic field, equally spaced around a circular path and each Lorentz factor $\gamma = 5$. As the number of electron tends to infinity no radiation is emitted. The power radiated has been averaged over 10 oscillations to demonstrate only harmonics of the cyclotron frequency are emitted. In Figure 3.3b we have also plotted the analytic solutions from Figure 3.1b, to show even harmonics are coherent and scale with N_p^2. Analytic solutions are provided by equation (3.18).

Chapter 4

Spin precession in a monochromatic plane wave

So far we have successfully demonstrated that our numerical code accurately predicts the electron trajectory, energy spectrum and spin precession against analytic solutions, for a constant magnetic field. As described in the introduction, we are predominantly interested with electrons initially counter propagating with a laser pulse, which we might approximate as a plane wave. Ideally we would solve the BMT equation (1.4) for a plane wave pulse, however this is non-trivial. To develop an intuition for this problem we will instead consider the spin precession in a linearly polarised monochromatic plane wave, for which the BMT equation can easily be solved. Throughout this chapter we will frequently reference the general equations of motion for an electron in a plane wave, derived in Appendix B. In this chapter we have neglected to simulate the energy emitted, because this would only be superseded by our consideration of a more physically realistic, linearly polarised plane wave pulse in the next chapter.

4.1   Solution of the Bargmann-Michel-Telegdi equation

Consider a single electron in a monochromatic plane wave with frequency ω_0. The wave is propagating along the $\hat{z}$ axis, and initially so is the electron. We can write the phase of this electron as,

$$\varphi(t) = \omega_0 \left[t - z(t) \right], \qquad \frac{d\varphi}{dt} = \frac{\omega_0 \delta}{\gamma(\varphi)}. \tag{4.1}$$

The derivative of φ is defined in the Appendix (B.10), and we have made use of the conserved quantity $\delta = \gamma(\varphi) - u_z(\varphi) = \gamma_0 - u_{0z}$ (B.9). Quantities like momentum and the Lorentz factor with a zero subscript are defined at the origin at time $t = 0$, or equivalently $\varphi = 0$. Using the differential relation between phase and time, we can rewrite the BMT equation (2.22),

$$\frac{d\boldsymbol{s}}{d\varphi} = \frac{\gamma(\varphi)}{\delta \, \omega_0} \, \boldsymbol{\Omega}(\varphi) \times \boldsymbol{s}(\varphi),$$

$$\boldsymbol{\Omega}(\varphi) = \left(a_e + \frac{1}{\gamma(\varphi)} \right) \boldsymbol{B}(\varphi) - \left(a_e + \frac{1}{\gamma(\varphi) + 1} \right) \frac{\boldsymbol{u}(\varphi) \times \boldsymbol{E}(\varphi)}{\gamma(\varphi)}$$
$$- \frac{a_e}{\gamma(\varphi) + 1} \left(\frac{\boldsymbol{u}(\varphi) \cdot \boldsymbol{B}(\varphi)}{\gamma(\varphi)} \right) \boldsymbol{u}(\varphi). \tag{4.2}$$

Now we can specify a simple sinusoidal vector potential, polarised along $\hat{\boldsymbol{x}}$. For convenience we always normalise the potential relative to the electron charge and mass (A.4). The momentum can be derived by inserting the potential (4.3a) into the generic equations of motion for an electron in a plane wave, as defined in the Appendix (B.14);

$$\boldsymbol{a}(\phi) = a_0 \sin{(\varphi)}\, \hat{\boldsymbol{x}}, \tag{4.3a}$$
$$u_x(\varphi) = a_0 \sin(\varphi), \tag{4.3b}$$
$$u_y(\varphi) = 0, \tag{4.3c}$$
$$u_z(\varphi) = u_{0z} + \frac{a_0^2}{2\delta} \sin^2(\varphi). \tag{4.3d}$$

From this vector potential the fields can be defined in the usual way $e\boldsymbol{B}/m_e = \nabla_{\boldsymbol{r}} \times \boldsymbol{a}$ and $e\boldsymbol{E}/m_e = \partial_t \boldsymbol{a}$ (A.5). One can immediately see this scenario is not physical. The acceleration or electromagnetic fields are 'turned on' at the beginning of the simulation $\varphi = 0$, and are therefore discontinuous. A better argument would be to insert an envelope function $f(\varphi)$ into our vector potential (4.3a), then define our initial conditions at some integer number of oscillations $\varphi = -N\pi$ yielding the same initial conditions above $\boldsymbol{u}(-N\pi) = u_{0z}$. One could then take the limit $N \to \infty$ where the envelope is expected to be zero if finite in duration, $f(-\infty) = 0$. Then we could approximate the envelope as constant when integrating, if it is very slowly varying. This is the formal argument one should give to derive the results found in this section. Using the potential from equation (4.3a) and its corresponding fields, with the momentum defined in equations (4.3b), (4.3c) and (4.3d) we can find the field dependent vector $\boldsymbol{\Omega}$ (4.2),

$$\Omega_y(\varphi) = -\frac{\delta \omega_0 a_0 \cos(\varphi)}{\gamma(\varphi)} \left[a_e + \frac{2(\delta + 1)}{(\delta + 1)^2 + a_0^2 \sin^2(\varphi)} \right]. \tag{4.4}$$

Written in terms of the conserved quantity δ. Due to our choice of potential and initial momentum the other components are zero which greatly simplifies this problem: $\Omega_x = 0$, $\Omega_z = 0$. Choosing these parameters allows us to ignore any movement parallel to the magnetic field (which is linear and not interesting) or in the wave polarisation direction. Expanding out the cross product in equation (4.2), the differential equations for spin are:

$$\frac{ds_x}{d\varphi} = \frac{\gamma(\varphi)}{\delta\,\omega_0} \Omega_y(\varphi)\, s_z(\varphi), \tag{4.5a}$$
$$\frac{ds_y}{d\varphi} = 0, \tag{4.5b}$$
$$\frac{ds_z}{d\varphi} = -\frac{\gamma(\varphi)}{\delta\,\omega_0} \Omega_y(\varphi)\, s_x(\varphi). \tag{4.5c}$$

The spin component s_y parallel to the magnetic field is conserved. By taking the scalar product of the BMT equation (4.2) with s we can show the total spin $s_x^2 + s_y^2 + s_z^2$ is conserved (phase dependence here is implied). With these two facts we can relate s_x and s_z by a simple constant s,

$$\frac{d}{d\varphi}\left([s_x(\varphi)]^2 + [s_z(\varphi)]^2\right) = 0, \qquad [s_x(\varphi)]^2 + [s_z(\varphi)]^2 = s_{0x}^2 + s_{0z}^2 = s^2. \tag{4.6}$$

By differentiating this the expression we can relate the derivatives of s_x and s_z, which allows us to obtain an ordinary differential equation for a single spin component,

$$\frac{ds_z}{d\varphi} = \frac{d}{d\varphi}\sqrt{s^2 - [s_x(\varphi)]^2} = -\frac{s_x(\varphi)}{\sqrt{s^2 - [s_x(\varphi)]^2}}\frac{ds_x}{d\varphi}. \tag{4.7}$$

Then by equating with (4.5c),

$$\int \frac{ds_x}{\sqrt{s^2 - [s_x(\varphi)]^2}} = \int \frac{\gamma(\varphi)\Omega_y(\varphi)}{\delta\,\omega_0}\,d\varphi. \tag{4.8}$$

Substituting in our equation for Ω_y (4.4), one can see these are standard integrals;

$$\sin^{-1}\left(\frac{s_x}{s}\right) = -a_0 a_e \int \cos(\phi)\,d\phi - 2\int \frac{dx}{1 + x^2}, \qquad \text{where} \quad x = \frac{a_0\sin(\phi)}{\delta + 1}, \tag{4.9}$$

$$s_x(\varphi) = -s\,\sin\left(a_0 a_e \sin(\varphi) + 2\tan^{-1}\left[\frac{a_0\sin(\varphi)}{\delta + 1}\right] + c\right). \tag{4.10}$$

Where c is an integration constant. By using the conservation equation relating s_z to s_z (4.6), we can obtain the general solution for s_z,

$$s_z(\varphi) = \sqrt{s^2 - [s_x(\varphi)]^2} = s\,\cos\left(a_0 a_e \sin(\varphi) + 2\tan^{-1}\left[\frac{a_0\sin(\varphi)}{\delta + 1}\right] + c\right). \tag{4.11}$$

By expanding equations (4.10) and (4.11) out with compound angle formulae and applying the initial conditions for spin $s_x(\varphi = 0) = s_{x0}$ and $s_z(\varphi = 0) = s_{0z}$, we obtain $\sin(c) = -s_{0x}/s$ and $\cos(c) = s_{0z}/s$. Notice that the inverse tan function is undetermined up to some integer multiple of π, but shifting the trigonometric functions by an integer multiple of their period leaves them unchanged. After applying these initial conditions, our equations of motion for spin become;

$$s_x(\varphi) = s_{0x}\cos(\mathcal{I}[\varphi]) - s_{0z}\sin(\mathcal{I}[\varphi]), \tag{4.12a}$$

$$s_y(\phi) = s_{0y}, \tag{4.12b}$$

$$s_z(\varphi) = s_{0z}\cos(\mathcal{I}[\varphi]) + s_{0x}\sin(\mathcal{I}[\varphi]), \tag{4.12c}$$

$$\mathcal{I}(\varphi) = a_0 a_e \sin(\varphi) + 2\tan^{-1}\left(\frac{a_0\sin(\varphi)}{\delta + 1}\right). \tag{4.12d}$$

Finally we note that these solutions are exact, and while the initial values for momentum are not general, the initial values of spin are.

4.2 Comparison with simulation
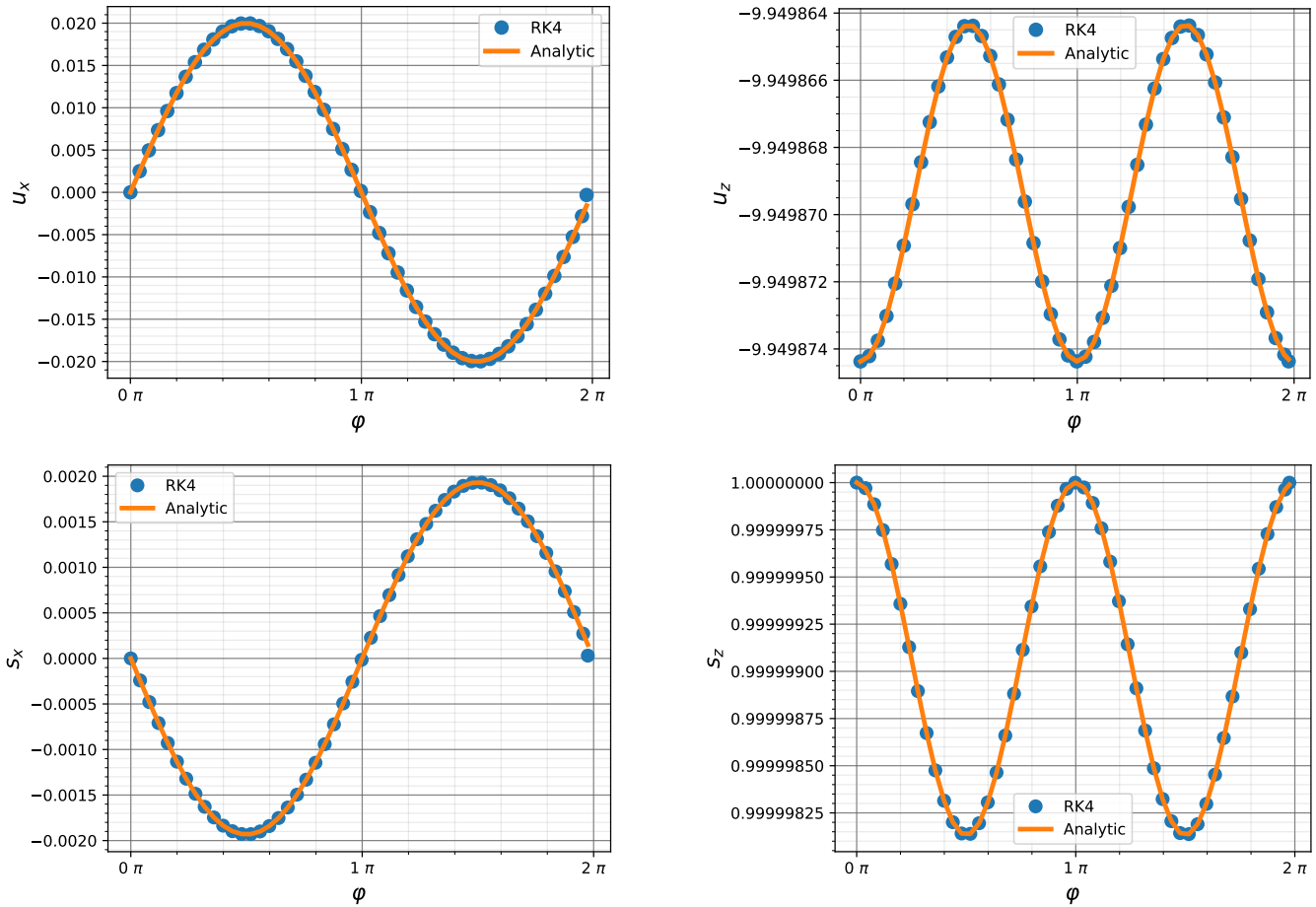
Figure 4.1: Spin precession in a single oscillation of a linearly polarised monochromatic plane wave (4.3a). Analytic solutions are provided in equations (4.3b) and (4.3d) for momentum, and equations (4.12a) and (4.12c) for spin.

As a monochromatic plane wave is somewhat unrealistic because of its infinite duration, we will not consider the energy radiated in this case; instead the reader can see chapter 5, which deals with a plane wave pulse. This means we no longer require a small time step to resolve high frequencies in the spectrum, which gives us an opportunity to demonstrate our code's accuracy with a small time step, $dt = \lambda_0/100c$ s in terms of the wavelength $\lambda_0 = 0.8$ μm. We select a dimensionless amplitude $a_0 = 0.02$, initial momentum $u_{0z} = -\sqrt{\gamma_0^2 - 1}$ with Lorentz factor $\gamma_0 = 10$ at the origin, and initial spin polarisation along the propagation axis $s_0 = (0, 0, 1)$. The results can be seen in Figure 4.1. In particular one can see a discrepancy at the last step for momentum and spin, u_x and s_x, in the plane of polarisation. As in the case of a constant magnetic field, both spin and momentum appear to oscillate with the same frequency, and any effect from the anomalous term a_e is small. This simple idea, that the electron spin is not significantly changed after an interaction with a plane wave, is the basis for generating relativistic, spin polarised electron beams from laser wake field acceleration. However with a more realistic laser pulse, as modelled in PIC simulations by Wen, Tamburini and Keitel there is a greater degree of depolarisation, demonstrated over many cycles [WTK19, Fig.2, (c) and (d)].

Chapter 5

Plane wave pulse

Another paradigmatic case to consider is radiation from an electron in the presence of a plane wave. This has been studied before in seminal papers by Sarachik and Schappert [SS70], Salamin and Faisal [SF96]. Sarachik and Schappert consider the average rest frame where the electron motion is periodic, and then proceed to solve the radiation integral (1.3) to obtain power radiated into the m th harmonic per unit solid angle, for a plane wave of arbitrary polarisation. Salamin and Faisal perform a similar derivation for a circularly polarised plane wave, which they then Lorentz transform to find the power radiated into the m th 'harmonic' in the lab frame. We wish to derive the appropriate conditions under which radiation from multiple electrons moving with the same initial velocity will constructively interfere. Throughout this chapter we will frequently reference the electron's equations of motion in a plane wave from Appendix B, and approximate solutions to the radiation integral in the case of a weak field from Appendix C.

5.1   Radiation integral of electrons in a generic plane wave pulse

Consider an electron denoted by j in the presence of a plane wave pulse. The wave is propagating along a direction specified by the dimensionless unit vector $\hat{\boldsymbol{n}}_0$. We can write the phase of each particle can be written as $\varphi_j(t) = \omega_0[t - \hat{\boldsymbol{n}}_0 \cdot \boldsymbol{r}_j(t)]$, for frequency ω_0. Such a wave can be described by the normalised vector potential (A.4),

$$\boldsymbol{a}(\varphi) = \begin{cases} 0 & \text{for } \varphi < \phi_i, \\ \boldsymbol{a}(\varphi) & \text{for } \phi_i \leq \varphi \leq \phi_f, \\ 0 & \text{for } \phi_f < \varphi. \end{cases} \tag{5.1}$$

When the phase is treated as a variable φ, particle subscript j is always implied. We require that potential $\boldsymbol{a}(\varphi)$ and its first derivative are both continuous and differential at all times; and are non-zero only between some initial and final phase $\phi_i \leq \varphi \leq \phi_f$. Aside from these conditions, the pulse shape and polarisation is completely general. All particles are assumed to start outside the pulse with initial phase $\phi_{0,j} = -\omega_0 \hat{\boldsymbol{n}}_0 \cdot \boldsymbol{r}_{0,j} \leq \phi_i$, where a zero subscript on a particle's momentum or position indicates it is defined at time $t = 0$. Defining the initial phase at $t = 0$ is an arbitrary choice, while starting at some other time simply introduces a constant phase for every particle which vanishes under the square modulus of the radiation integral (1.1). The equations of motion

can be derived in the lab frame using the Hamilton-Jacobi method, this procedure is laid out in Appendix B closely following common literature [SF96; SS70; LL75];

$$
\boldsymbol{u}_j(\varphi) = \begin{cases} \boldsymbol{u}_{0,j} & \text{for } \phi_{0,j} \leq \varphi < \phi_i, \\ \boldsymbol{u}_{0,j} + \boldsymbol{a}(\varphi) + \frac{1}{\delta_j}\left(\boldsymbol{u}_{0,j} \cdot \boldsymbol{a}(\varphi)\right)\hat{\boldsymbol{n}}_0 + \frac{1}{2\delta_j}\left[\boldsymbol{a}(\varphi)\right]^2 \hat{\boldsymbol{n}}_0 & \text{for } \phi_i \leq \varphi \leq \phi_f, \\ \boldsymbol{u}_{0,j} & \text{for } \phi_f < \varphi. \end{cases} \tag{5.2}
$$

$$
\omega_0(\boldsymbol{r}_j(\varphi) - \boldsymbol{r}_{0,j}) = \begin{cases} (\varphi - \phi_{0,j})\boldsymbol{u}_{0,j}/\delta_j & \text{for } \phi_{0,j} \leq \varphi < \phi_i, \\ \left[(\varphi - \phi_{0,j})\boldsymbol{u}_{0,j} + \boldsymbol{\Theta}_j(\phi_i, \varphi)\right]/\delta_j & \text{for } \phi_i \leq \varphi \leq \phi_f, \\ \left[(\varphi - \phi_{0,j})\boldsymbol{u}_{0,j} + \boldsymbol{\Theta}_j(\phi_i, \phi_f)\right]/\delta_j & \text{for } \phi_f < \varphi, \end{cases} \tag{5.3}
$$

$$
\boldsymbol{\Theta}_j(\phi_i, \varphi) = \int_{\phi_i}^{\varphi}\left(\boldsymbol{a}(\varphi') + \frac{1}{\delta_j}\left(\boldsymbol{u}_{0,j} \cdot \boldsymbol{a}(\varphi')\right)\hat{\boldsymbol{n}}_0 + \frac{1}{2\delta_j}\left[\boldsymbol{a}(\varphi')\right]^2 \hat{\boldsymbol{n}}_0\right)d\varphi'. \tag{5.4}
$$

Parameter delta $\delta_j = \gamma_j(\varphi) - \hat{\boldsymbol{n}}_0 \cdot \boldsymbol{u}_j(\varphi) = \gamma_{0,j} - \hat{\boldsymbol{n}}_0 \cdot \boldsymbol{u}_{0,j}$ is a conserved quantity defined by equation (B.9). When describing the structure of our numerical code we wrote the radiation integral in terms of the relativistic momentum $\boldsymbol{u}_j$ (2.16), which is stated again below for convenience. Substitution of our equations of motion (5.2) to (5.4) into this integral allows us to discern the properties of energy radiated in a plane wave of general structure;

$$
\frac{d^2 E}{d\omega d\Omega} = \frac{e^2}{16\pi^3}\left|\sum_j \int_{-\infty}^{\infty} \frac{\hat{\boldsymbol{n}} \times \left(\hat{\boldsymbol{n}} \times \left[\gamma_j^2 \dot{\boldsymbol{u}}_j - (\boldsymbol{u}_j \cdot \dot{\boldsymbol{u}}_j)\boldsymbol{u}_j\right] - \gamma_j \boldsymbol{u}_j \times \dot{\boldsymbol{u}}_j\right)}{\gamma_j(\gamma_j - \hat{\boldsymbol{n}} \cdot \boldsymbol{u}_j)^2} e^{i\omega[t - \hat{\boldsymbol{n}} \cdot \boldsymbol{r}_j]}dt\right|^2. \tag{5.5}
$$

A dot denotes a derivative with respect to time, and the time dependence of position $\boldsymbol{r}_j$, momentum $\boldsymbol{u}_j$ and Lorentz factor γ_j is implied. Since are considering motion in a generic plane wave pulse, it is convenient to change the variable of integration to the wave phase using the differential relation (B.10),

$$
\varphi_j(t) = \omega_0\left[t - \hat{\boldsymbol{n}}_0 \cdot \boldsymbol{r}_j(t)\right], \qquad \frac{d\varphi_j}{dt} = \frac{\omega_0 \delta_j}{\gamma_j(\varphi_j)}. \tag{5.6}
$$

Where we have included subscript j explicitly to show this change of variable must be performed for each particle. This technique was originally employed by Sarachik and Schappert [SS70]. By rewriting the integrand as a total differential in time using the following equation, analogous to an equation used earlier (1.2), allows us to remove the acceleration terms;

$$
\frac{d}{dt}\left(\frac{\hat{\boldsymbol{n}} \times [\hat{\boldsymbol{n}} \times \boldsymbol{u}_j]}{\gamma_j - \hat{\boldsymbol{n}} \cdot \boldsymbol{u}_j}\right) = \frac{\hat{\boldsymbol{n}} \times \left(\hat{\boldsymbol{n}} \times \left[\gamma_j^2 \dot{\boldsymbol{u}}_j - (\boldsymbol{u}_j \cdot \dot{\boldsymbol{u}}_j)\boldsymbol{u}_j\right] - \gamma_j \boldsymbol{u}_j \times \dot{\boldsymbol{u}}_j\right)}{\gamma_j(\gamma_j - \hat{\boldsymbol{n}} \cdot \boldsymbol{u}_j)^2}. \tag{5.7}
$$

Changing the variable of integration to phase for each particle j using equations eqs. (5.6) and (5.7) allows us to obtain the following radiation integral,

$$
\frac{d^2 E}{d\omega d\Omega} = \frac{e^2}{16\pi^3}\left|\sum_j \int_{-\infty}^{\infty} \frac{d}{d\varphi}\left(\frac{\hat{\boldsymbol{n}} \times [\hat{\boldsymbol{n}} \times \boldsymbol{u}_j(\varphi)]}{\gamma_j(\varphi) - \hat{\boldsymbol{n}} \cdot \boldsymbol{u}_j(\varphi)}\right) e^{i\Phi_j(\varphi)}d\varphi\right|^2, \tag{5.8}
$$

$$\Phi_j(\varphi) = \frac{\omega}{\omega_0}\left[\varphi + \omega_0(\hat{\boldsymbol{n}}_0 - \hat{\boldsymbol{n}}) \cdot \boldsymbol{r}_j(\varphi)\right]. \tag{5.9}$$

The energy radiated is identically zero for any interval in which the momentum is constant (5.8), as expected. Note the derivative of phase Φ_j is proportional to the Doppler factor of the particle,

$$\frac{d\Phi_j}{d\varphi} = \frac{\omega}{\omega_0}\left(\frac{\gamma_j(\varphi) - \hat{\boldsymbol{n}} \cdot \boldsymbol{u}_j(\varphi)}{\gamma_j(\varphi) - \hat{\boldsymbol{n}}_0 \cdot \boldsymbol{u}_j(\varphi)}\right) = \frac{\omega}{\delta_j\omega_0}\left[\gamma_j(\varphi) - \hat{\boldsymbol{n}} \cdot \boldsymbol{u}_j(\varphi)\right]. \tag{5.10}$$

Where we have used the differential relation between momentum and position from the Appendix (B.11). Carrying out integration by parts of equation (5.8) allows us to obtain a simpler radiation integral similar to equation (1.3),

$$\frac{d^2E}{d\omega d\Omega} = \frac{e^2\omega^2}{16\pi^3\omega_0^2}\left|\sum_j \frac{1}{\delta_j}\int_{-\infty}^{\infty} \hat{\boldsymbol{n}} \times (\hat{\boldsymbol{n}} \times \boldsymbol{u}_j(\varphi))\ e^{i\Phi_j(\varphi)}d\varphi\right|^2. \tag{5.11}$$

The argument for dispensing with the boundary terms was given in the introduction for equation (1.3); one assumes the motion is periodic, integrates over an integer number of oscillations, considers radiation only at harmonics and sends the time period of oscillation to infinity. There are similar assumptions used in literature [Jac98; RK10]. One could correctly argue that electron motion in a plane wave is not in general periodic in the laboratory frame, and that the boundary conditions should not be discarded. However they have no impact on this derivation, so it is not necessary to include them.

5.2 Interference conditions for two electrons with identical initial velocity

Our goal is to derive some condition for constructive interference. We expect the frequency of emitted radiation to depend on the Doppler factor of each electron, and therefore its initial momentum. It is natural to start by requiring the initial momentum of all particles to be identical for interference; in doing so we drop the j subscript from δ_j, γ_j and $\boldsymbol{u}_j$ (5.2). This indicates that Θ_j (5.4) is also independent of particle, so we drop the subscript j here also. Only the position $\boldsymbol{r}_j(\varphi)$ varies for each particle. Substituting the momentum $\boldsymbol{u}(\varphi)$ (5.2) and position $\boldsymbol{r}_j(\varphi)$ (eqs. (5.3) and (5.4)) into our equation for phase Φ_j (5.9) we obtain,

$$\Phi_j(\varphi) = \frac{\omega}{\omega_0}\left[(\hat{\boldsymbol{n}}_0 - \hat{\boldsymbol{n}}) \cdot (\omega_0\boldsymbol{r}_{0,j} - \frac{\phi_{0,j}}{\delta}\boldsymbol{u}_0) + \left(1 + \frac{1}{\delta}[\hat{\boldsymbol{n}}_0 - \hat{\boldsymbol{n}}] \cdot \boldsymbol{u}_0\right)\varphi + \frac{1}{\delta}(\hat{\boldsymbol{n}}_0 - \hat{\boldsymbol{n}}) \cdot \boldsymbol{\Theta}(\phi_i, \varphi)\right], \tag{5.12}$$

in the interval where the potential is non-zero $\phi_i \leq \varphi \leq \phi_f$. Here Φ_j can be split into two parts, a constant which depends on the initial position of each particle and a variable independent of the particle. Using this, we can restate the radiation integral such that it no longer depends on the choice of particle. Substituting the momentum $\boldsymbol{u}$ (5.2) and phase Φ_j (5.12) into the radiation integral (5.11),

$$\frac{d^2E}{d\omega d\Omega} = \frac{e^2\omega^2}{16\pi^3\delta^2\omega_0^2} \; F\left(\omega\right) \; \left| \int_{\phi_i}^{\phi_f} \hat{\boldsymbol{n}} \times \left(\hat{\boldsymbol{n}} \times \boldsymbol{u}(\varphi)\right) \; e^{i\frac{\omega}{\omega_0}\left[\varphi + \frac{1}{\delta}(\hat{\boldsymbol{n}}_0-\hat{\boldsymbol{n}})\cdot\left(\varphi\boldsymbol{u}_0 + \boldsymbol{\Theta}(\phi_i,\varphi)\right)\right]} \, d\varphi \right|^2. \qquad (5.13)$$

Here the limits of integration are restricted to the region in which the acceleration is non-zero (5.8). The dependence on particles' initial positions is given by the following sum of constant phase terms

$$F\left(\omega\right) = \left| \sum_{j=0}^{N_p-1} e^{i\omega(\sigma\hat{\boldsymbol{n}}_0-\hat{\boldsymbol{n}})\cdot\boldsymbol{r}_{0,j}} \right|^2 \qquad \text{where } \sigma = \frac{\gamma_0 - \hat{\boldsymbol{n}}\cdot\boldsymbol{u}_0}{\gamma_0 - \hat{\boldsymbol{n}}_0\cdot\boldsymbol{u}_0}. \qquad (5.14)$$

This sum is similar to one obtained earlier in the specific case of a constant magnetic field (3.18); we have shown this behaviour can be generalised to any plane wave pulse. If the emission is coherent at a certain frequency ω then the energy radiated will scale with the number of electrons squared; $F(\omega) = N_p^2$, where N_p is the total number of particles. Parameter σ has been derived by inserting the initial phase $\phi_{0,j} = -\omega_0\hat{\boldsymbol{n}}_0\cdot\boldsymbol{r}_{0,j}$ into equation (5.12) and rearranging, it is similar to the square of a Doppler factor. This result no longer depends explicitly on the frequency ω_0, and perhaps most importantly equation (5.14) is general and makes no references to the pulse structure.

Consider just two particles ($j = 1, 2$), both with initial momenta $\boldsymbol{u}_0$. Expanding out the sum (5.14), we can see the general condition for observing coherent radiation is,

$$\omega \left(\left[\frac{\gamma_0 - \hat{\boldsymbol{n}}\cdot\boldsymbol{u}_0}{\gamma_0 - \hat{\boldsymbol{n}}_0\cdot\boldsymbol{u}_0} \right] \hat{\boldsymbol{n}}_0 - \hat{\boldsymbol{n}} \right) \cdot \boldsymbol{d} = 2\pi l. \qquad (5.15)$$

Where the displacement of one electron from another is $\boldsymbol{d} = \boldsymbol{r}_{0,2} - \boldsymbol{r}_{0,1}$ with distance $d = |\boldsymbol{d}|$, the sign on $\boldsymbol{d}$ is irrelevant as l is an integer (positive or negative). Clearly the condition for coherent radiation varies with the direction of observation and frequency. To simplify this condition, we require the observation direction $\hat{\boldsymbol{n}}$, propagation direction of the wave $\hat{\boldsymbol{n}}_0$ and displacement of the electrons to be co-planar. The angle between the observation direction $\hat{\boldsymbol{n}}$ and wave propagation direction $\hat{\boldsymbol{n}}_0$ is ϑ. First we assume both electrons are transversely separated $\boldsymbol{d}_\perp \cdot \hat{\boldsymbol{n}}_0 = 0$, then we can determine angles $\vartheta_\perp$ at which coherent radiation is detected for a given frequency, or we can determine frequencies $\omega_\perp$ at which coherent radiation is detected for a given angle. The same procedure is repeated for separation parallel to the propagation direction $\boldsymbol{d}_\parallel \times \hat{\boldsymbol{n}}_0 = 0$. Using equation (5.15) conditions for coherent radiation are:

$$\vartheta_\perp(\omega) = \sin^{-1}\left(\frac{2\pi l}{d_\perp \omega} \right), \qquad (5.16)$$

$$\omega_\perp(\vartheta) = \frac{2\pi l}{d_\perp \sin(\vartheta)}, \qquad (5.17)$$

$$\vartheta_\parallel(\omega) = \cos^{-1}\left(\frac{\gamma_0 - \hat{\boldsymbol{n}}\cdot\boldsymbol{u}_0}{\gamma_0 - \hat{\boldsymbol{n}}_0\cdot\boldsymbol{u}_0} + \frac{2\pi l}{d_\parallel \omega} \right), \qquad (5.18)$$

$$\omega_{\parallel}(\vartheta) = \frac{2\pi l}{d_{\parallel}\left[\left(\dfrac{\gamma_0 - \hat{\boldsymbol{n}} \cdot \boldsymbol{u}_0}{\gamma_0 - \hat{\boldsymbol{n}}_0 \cdot \boldsymbol{u}_0}\right) - \cos(\vartheta)\right]}. \tag{5.19}$$

The sign on integer l is not consistent from one equation to another, and taking l instead as a half integer would give destructive interference. There are a few interesting comments to make here. Quantities $\vartheta_{\parallel}$ and $\omega_{\parallel}$ depend on the Doppler factor while $\vartheta_{\perp}$ and $\omega_{\perp}$, strangely do not. Coherence is observed at every frequency $\omega_{\perp}$ along the wave propagation direction $\vartheta = 0$. This un-physical behaviour may be a result of the plane wave approximation, as two far away electrons should not radiate coherent light. Recall that in deriving the radiation integral (1.1), Jackson approximated $\hat{\boldsymbol{n}}$ as constant for far away observers. So radiation from two electrons could be considered loosely analogous to a double slit experiment with a far away screen.

5.3   Testing interference conditions for a linearly polarised pulse

In previous sections, we considered the energy radiated from multiple electrons in the presence of a plane wave of general shape, and derived conditions for coherent emission. We want to test these conditions using both our numerical code, and approximate analytic solutions. To begin, we consider the following normalised vector potential for a plane wave pulse, linearly polarised along $\hat{\boldsymbol{x}}$ and propagating along $\hat{\boldsymbol{z}}$;

$$\boldsymbol{a}(\varphi) = \begin{cases} 0 & \text{for } \varphi < -L\pi, \\ a_0 \cos(\varphi) \cos^2\left(\frac{\varphi}{2L}\right) \hat{\boldsymbol{x}} & \text{for } -L\pi \leq \varphi \leq L\pi, \\ 0 & \text{for } L\pi < \varphi. \end{cases} \tag{5.20}$$

The phase for each particle j is similar to the previous section, $\varphi_j(t) = \omega_0[t - \hat{\boldsymbol{z}} \cdot \boldsymbol{r}_j(\varphi)]$, and we will continue to suppress the particle index on the variable phase φ for convenience. L is an integer defining the half width of the envelope.

At this point we would proceed to state the momentum of each particle and integrate to find position using the general equations of motion for electrons in a plane wave (see Appendix B). With this information, we could then solve the radiation integral in terms of the phase (5.11). The resulting radiation integral depends on several infinite series of Bessel functions of the first kind, as originally shown by Sarachik and Schappert for a monochromatic plane wave [SS70]. In the case of a linearly polarised wave this cannot be solved exactly. However in the simplified case of a weak field $a_0 \ll 1$ for frequencies in the order of $\omega = 4\gamma_0^2\omega_0$ and below, we have derived an approximate solution in Appendix C. The full procedure is lengthy so we will only state the key results here.

Substituting the normalised vector potential $\boldsymbol{a}(\varphi)$ (5.20) into our equation for momentum in a plane wave (5.2) while ignoring oscillations along the wave propagation axis for weak fields $a_0 \ll 1$, we can obtain equation (C.3)

$$\boldsymbol{u}_j(\varphi) \approx \boldsymbol{u}_{0,j} + a_0 \left(\hat{\boldsymbol{x}} + \frac{\hat{\boldsymbol{x}} \cdot \boldsymbol{u}_{0,j}}{\delta_j} \hat{\boldsymbol{z}}\right) \cos(\varphi) \cos^2\left(\frac{\varphi}{2L}\right). \tag{5.21}$$

For an electron denoted by j while interacting with the pulse, $-L\pi \leq \varphi \leq L\pi$. Electron properties

such as position $\boldsymbol{r}_{0,j}$ and momentum $\boldsymbol{u}_{0,j}$ subscripted by a zero are determined at the initial phase $\phi_{0,j} = -\omega_0 \hat{\boldsymbol{z}} \cdot \boldsymbol{r}_{0,j} < -L\pi$, where all particles start outside the pulse. The conserved quantity delta is defined by $\delta_j = \gamma_j(\varphi) - \hat{\boldsymbol{z}} \cdot \boldsymbol{u}_j(\varphi) = \gamma_{0,j} - \hat{\boldsymbol{z}} \cdot \boldsymbol{u}_{0,j}$, as derived in the Appendix (B.9). We can integrate the momentum with respect to phase (B.12), to obtain the approximate position (C.4)

$$
\begin{aligned}
\omega_0(\boldsymbol{r}_j(\varphi) - \boldsymbol{r}_{0,j}) \approx {}& \frac{\boldsymbol{u}_{0,j}}{\delta_j}(\varphi - \phi_{0,j}) \\
& + \frac{a_0}{4\delta_j}\left(\hat{\boldsymbol{e}} + \frac{\hat{\boldsymbol{x}} \cdot \boldsymbol{u}_{0,j}}{\delta_j}\hat{\boldsymbol{z}}\right)\left(2\sin(\varphi) + \frac{\sin([1 - L^{-1}]\varphi)}{1 - L^{-1}} + \frac{\sin([1 + L^{-1}]\varphi)}{1 + L^{-1}}\right).
\end{aligned}
\tag{5.22}
$$

After substitution of the momentum and position into the radiation integral (C.5), with much simplification one can obtain the total energy radiated per unit frequency, per unit solid angle from an arbitrary number of particles during their interaction with the pulse. From equations (C.7) and (C.27) we can write this as

$$
\frac{d^2E}{d\omega d\Omega} = \frac{e^2 L^2 \omega^2}{4\pi\omega_0}\left|\sum_j \boldsymbol{K}_j\right|^2,
\tag{5.23}
$$

$$
\begin{aligned}
\boldsymbol{K}_j \approx {}& \frac{1}{\delta_j}e^{i\frac{\omega}{\omega_0}\lambda_j}\Bigg\{\hat{\boldsymbol{n}} \times (\hat{\boldsymbol{n}} \times \boldsymbol{u}_{0,j})\Bigg(J_1\left(2\rho_j\frac{\omega}{\omega_0}\right)\left[\operatorname{sinc}\left(\left[\frac{\omega}{\omega_0}\sigma_j + 1\right]L\pi\right) - \operatorname{sinc}\left(\left[\frac{\omega}{\omega_0}\sigma_j - 1\right]L\pi\right)\right] \\
& + J_1\left(\frac{\omega\rho_j}{\omega_0(1 + L^{-1})}\right)\left[\operatorname{sinc}\left(\left[\frac{\omega}{\omega_0}\sigma_j + 1 + L^{-1}\right]L\pi\right) - \operatorname{sinc}\left(\left[\frac{\omega}{\omega_0}\sigma_j - 1 - L^{-1}\right]L\pi\right)\right] \\
& + J_1\left(\frac{\omega\rho_j}{\omega_0(1 - L^{-1})}\right)\left[\operatorname{sinc}\left(\left[\frac{\omega}{\omega_0}\sigma_j + 1 - L^{-1}\right]L\pi\right) - \operatorname{sinc}\left(\left[\frac{\omega}{\omega_0}\sigma_j - 1 + L^{-1}\right]L\pi\right)\right]\Bigg) \\
& + \frac{a_0}{4}\left[\hat{\boldsymbol{n}} \times (\hat{\boldsymbol{n}} \times \hat{\boldsymbol{x}}) + \frac{\hat{\boldsymbol{x}} \cdot \boldsymbol{u}_{0,j}}{\delta_j}\hat{\boldsymbol{n}} \times (\hat{\boldsymbol{n}} \times \hat{\boldsymbol{z}})\right]\Bigg[\operatorname{sinc}\left(\left[\frac{\omega}{\omega_0}\sigma_j + 1\right]L\pi\right) + \operatorname{sinc}\left(\left[\frac{\omega}{\omega_0}\sigma_j - 1\right]L\pi\right) \\
& + \frac{1}{2}\operatorname{sinc}\left(\left[\frac{\omega}{\omega_0}\sigma_j + 1 + L^{-1}\right]L\pi\right) + \frac{1}{2}\operatorname{sinc}\left(\left[\frac{\omega}{\omega_0}\sigma_j - 1 - L^{-1}\right]L\pi\right) \\
& + \frac{1}{2}\operatorname{sinc}\left(\left[\frac{\omega}{\omega_0}\sigma_j + 1 - L^{-1}\right]L\pi\right) + \frac{1}{2}\operatorname{sinc}\left(\left[\frac{\omega}{\omega_0}\sigma_j - 1 + L^{-1}\right]L\pi\right)\Bigg]\Bigg\},
\end{aligned}
\tag{5.24}
$$

$$
\text{where} \qquad \operatorname{sinc}(x) = \frac{sin(x)}{x}.
$$

Our result has been stated in terms of various constants; σ_j (C.12a) is a Doppler factor, ρ_j (C.12c) depends on the field amplitude a_0 and the direction of observation $\hat{\boldsymbol{n}}$ relative to the polarisation plane $\hat{\boldsymbol{x}}$ and wave propagation direction $\hat{\boldsymbol{z}}$. Here λ_j (C.12b) is the exponent of the constant phase terms defined when deriving the general interference conditions (5.14). Each of these constants is stated below:

$$
\sigma_j = \frac{\gamma_{0,j} - \hat{\boldsymbol{n}} \cdot \boldsymbol{u}_{0,j}}{\gamma_{0,j} - \hat{\boldsymbol{z}} \cdot \boldsymbol{u}_{0,j}} = \frac{1}{\delta_j}\left(\gamma_{0,j} - \hat{\boldsymbol{n}} \cdot \boldsymbol{u}_{0,j}\right),
\tag{5.25a}
$$

$$\lambda_j = \omega_0(\sigma_j\hat{z} - \hat{n}) \cdot r_{0,j}, \tag{5.25b}$$

$$\rho_j = \frac{a_0}{4\delta_j}(\hat{z} - \hat{n}) \cdot \left(\hat{x} + \frac{\hat{x} \cdot u_{0,j}}{\delta_j}\hat{z}\right). \tag{5.25c}$$

For a finite number of particles we could expand out the square modulus of equation (5.24) to obtain a lengthy expression. Instead we have written a Python script which evaluates the radiation integral for some frequency ω and direction of observation $\hat{n}$, given the initial position and momentum of every particle. All Bessel functions of the first kind $J_n(x)$ are calculated to a high degree of accuracy with the Scipy package [Vir+20]. There are some observations we can make about this result. From equation (5.23) we can see the energy radiated is proportional to the length of the pulse squared. Inside the square modulus (5.24), we see a series of overlapping sinc functions centred on frequency $\omega = \omega_0/\sigma_j$; for reflected radiation from a relativistic particle one can show $1/\sigma_j \approx 4\gamma_{0,j}^2$. Taking the limit of a monochromatic plane wave $L \to \infty$ reduces every sinc function to a Dirac delta distribution $\delta(\omega - \omega_0/\sigma_j)$, restricting emission to a single Doppler shifted frequency. Clearly this limit can only be applied when integrating equation (5.23) over frequency, providing all other functions are smoothly varying.

Unless stated otherwise, we will always consider electrons counter propagating to a pulse given by equation (5.20) with amplitude $a_0 = 0.02$. The initial momentum will be identical for every particle along the $\hat{z}$ axis, $u_{0z} = -\sqrt{\gamma_0^2 - 1}\ \hat{z}$ corresponding to Lorentz factor $\gamma_0 = 10$. In light of this we have suspended all use of the particle subscript j on the momentum. The pulse half length will be $L = 10$, and the frequency of the rapid oscillations $\omega_0 = 2\pi c/\lambda_0$ is written in terms of the wavelength $\lambda_0 = 0.8$ μm. In practice our results will frequently be stated in terms of these parameters.

5.3.1 Single electron: equations of motion and spectrum

As stated in the previous section, to solve the radiation integral we ignored electron oscillations along the wave propagation axis providing $a_0 \ll 1$. It is worth checking the validity of this approximation. To this end we have performed a simulation for one electron counter propagating to a pulse given by equation (5.20), the results can be seen in Figure 5.1. Also plotted in Figure 5.1 are the approximate analytic solutions for momentum (5.21) and position (5.22), which have been used to calculate an approximate solution to the radiation integral given by equations (5.23) and (5.24), which is plotted with the energy spectrum. ϑ in Figure 5.1 refers to the angle between the direction of observation $\hat{n}$ and the direction in which the plane wave propagates, so $\vartheta = \pi$ is parallel to the initial electron momentum u_{0z}.

From Figure 5.1 one can see the approximate solutions accurately predict the momentum and trajectory in the plane of polarisation. Along the axis of propagation, our analytic solutions ignore small oscillations in the momentum, however this still accurately predicts the trajectory over large changes in the phase φ. If one wanted to check the legitimacy of our numerical code, substituting the normalised vector potential (5.20) into our general equations for momentum in a plane wave (B.14) produces a result indistinguishable from the numerical calculation for u_z. The main contribution to our approximate analytic solution for the spectrum (5.24) is a sinc function located at the Doppler shifted frequency, using this we can predict the location of the peak as a function of angle

$$\frac{\omega_{\mathsf{max}}}{\omega_0} = \frac{\gamma_0 - \hat{n}_0 \cdot u_0}{\gamma_0 - \hat{n} \cdot u_0} = \frac{\gamma_0 - u_{0z}}{\gamma_0 - u_{0z}\cos(\vartheta)}. \tag{5.26}$$
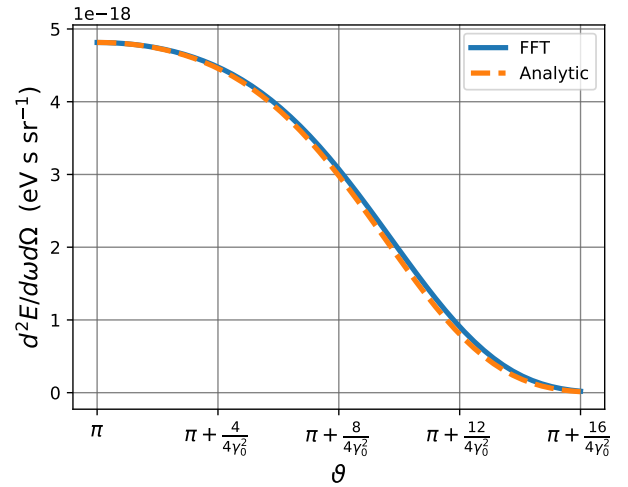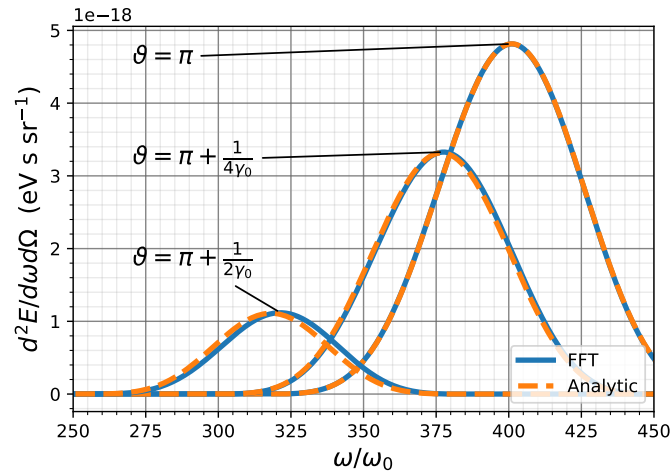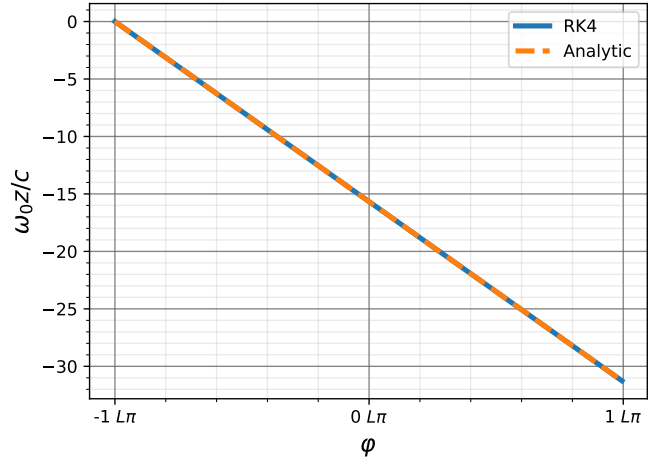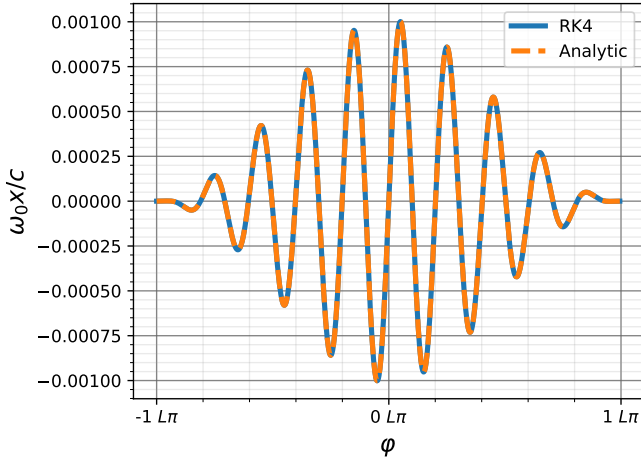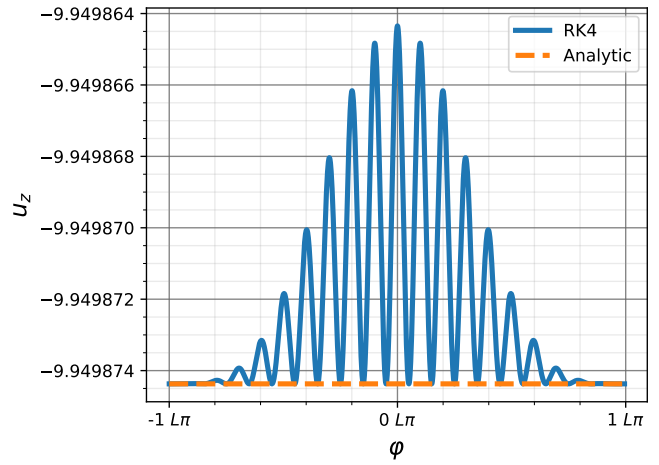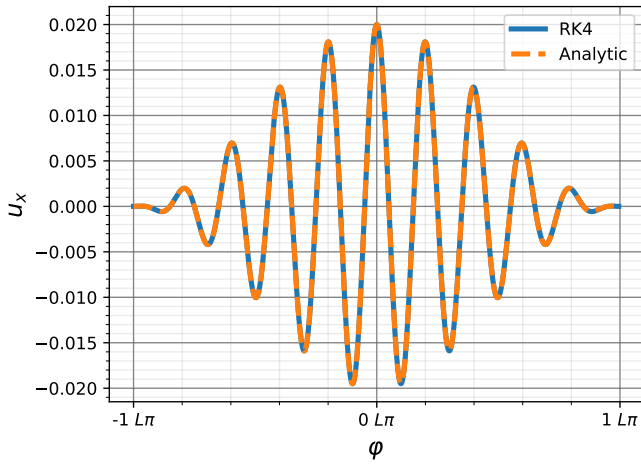
(a) Variation with frequency.

(b) Variation with angle, at $\omega = 4\gamma_0^2\omega_0$.

Figure 5.1: The momentum, trajectory and energy radiated from a single electron with Lorentz factor $\gamma_0 = 10$ counter propagating with a plane wave pulse. Each plot shows our numerical code against the approximate analytic solutions given in Appendix C. ϑ is the angle between the observation direction and wave propagation direction, while $\vartheta = \pi$ is parallel to the initial velocity.

Equation (5.26) accurately predicts the peak locations at approximately $398\omega_0$, $375\omega_0$ and $319\omega_0$ for angles $\vartheta = \pi$, $\pi + 1/4\gamma_0$, $\pi + 1/2\gamma_0$ respectively. These angles have been chosen as we expect most radiation from a relativistic particle to be emitted in a cone of full angle $\sim 1/\gamma_0$ around the velocity [LL75, § 73]. In Figure 5.1a we can see a discrepancy between numerical and analytic solutions at large angles from $\varphi = \pi$. This deviation results from an approximation made in deriving our analytic solutions; in Appendix C we assume observation only occurs at small angles around the initial momentum (close to $\vartheta = \pi$), such that the arguments of our Bessel functions are small, and we can truncate any series of Bessel functions. Equation (5.26) is similar to a result obtained by Salamin and Faisal for the first 'harmonic' in the lab frame [SF96, eq. 49]. They calculate the radiation integral in the average rest frame of the electron, where its motion is periodic and only harmonics are emitted in an infinitely long plane wave. Then they perform a Lorentz transformation back to the laboratory frame, and in this process the frequency of the harmonics pick up an angular dependence. Our approximate method in Appendix C ignores oscillations along the wave propagation axis, so we make no distinction between the average rest frame and the rest frame corresponding to the initial momentum, this discrepancy is why our results differ slightly to those of Salamin and Faisal.

5.3.2 Interference between two transversely separated electrons

In the previous section we accurately predicted the frequencies at which peak energy emission occurs, as a function of the observation angle ϑ relative to the wave propagation direction for one electron. When considering multiple electrons, we would like an electron distribution which produces constructive interference at these peaks. For example, consider two electrons with the same initial momentum u_{0z} as before, with identical z coordinates, separated by one wavelength $d_\perp = \lambda_0$ along the polarisation direction $\hat{x}$. We know the frequency at which the energy peaks occur for one electron from equation (5.26), and we can equate this to our condition for constructive interference $\omega_\perp(\vartheta)$ (5.17), and solve for angles of observation ϑ. Using compound angle formulae we can write the angles at which coherent radiation is detected

$$\vartheta(l) = \pi + \sin^{-1}\left(\frac{l\gamma_0}{\sqrt{(\gamma_0 - u_{0z})^2 + l^2 u_{0z}^2}}\right) + \tan^{-1}\left(\frac{l u_{0z}}{\gamma_0 - u_{0z}}\right) \qquad \text{for integer } l. \qquad (5.27)$$

Clearly the solutions for $\vartheta(l)$ are periodic, but we are only interested in reflected radiation near $\vartheta = \pi$, so equation (5.27) has been written assuming the inverse sine and tangent are solved in the closed interval $[-\pi/2, \pi/2]$. Equation (5.27) is only valid for a limited number of integers l, for which the argument of inverse sine is between minus one and one. A simulation has been performed with these parameters for angles $\vartheta(l = 0) = \pi$ and $\vartheta(l = 12) \approx \pi + 0.0335$, as shown in Figure 5.2a. Approximate analytic solutions for the radiation integral from equations (5.23) and (5.24), have been plotted for two electrons transversely separated, and one electron propagating along the axis. This allows us to see emission is indeed coherent at each peak determined by these angles, as it scales with the number of particles squared compared to the one electron case.

Radiation emitted is not coherent at every angle of observation. For example, if we fix our frequency at the Doppler shifted value $\omega = 4\gamma_0^2$, and solve our interference condition $\vartheta_\perp(\omega)$ (5.16) for small angles around $\vartheta = \pi$, our condition for constructive interference becomes $\vartheta \approx l/4\gamma_0^2$ for integer l. For relativistic particles this produces a rapidly varying interference pattern, seen

in Figure 5.2b. This can be contrasted with the one electron case where the radiation emitted decreases slowly with angle.

(a) Variation with frequency.

(b) Variation with angle, at $\omega = 4\gamma_0^2\omega_0$.
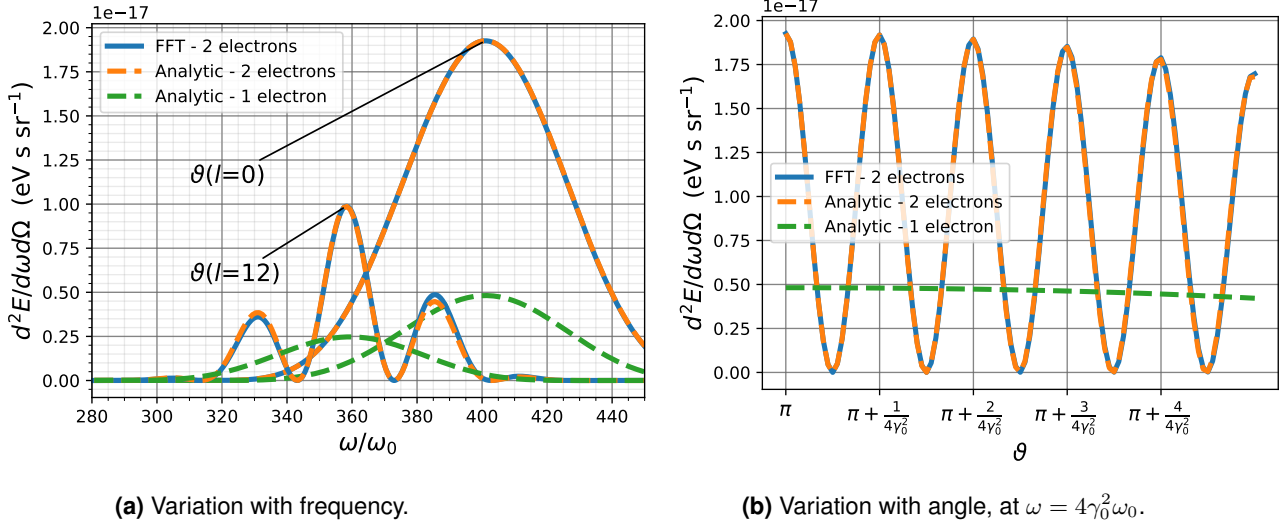
Figure 5.2: Energy radiated from two electrons with Lorentz factor $\gamma_0 = 10$, transversely separated by one wavelength, counter propagating with a plane wave pulse. Figure 5.2a shows the energy radiated varying with frequency, at angles were constructive interference can be seen. These angles are determined by evaluating equation (5.27) for integers $l = 0, 12$. Figure 5.2b shows the variation of energy radiated with small angles around the initial velocity, at the Doppler reflected frequency. ϑ is the angle between the observation direction and wave propagation direction, while $\vartheta = \pi$ is parallel to the initial velocity.

5.3.3 Interference between two longitudinally separated electrons

Consider two electrons initially moving with the same momentum u_{0z} and separated longitudinally by distance $d_\parallel$, along the wave propagation axis. For this case we have derived conditions which determine if constructive interference is observed at certain frequencies $\omega_\parallel$, and angles $\vartheta_\parallel$ relative to the wave propagation direction, given by equations (5.18) and (5.19). Our electrons are relativistic, so we expect most radiation to be emitted in a cone of full angle $\sim 1/\gamma_0$ around the momentum [LL75, § 73].

The interference condition for frequency $\omega_\parallel(\vartheta)$ (5.19) depends on angle ϑ only through cosine terms, which we can approximate as one to first order for small angles around the momentum $\vartheta = \pi$, within the radiation cone. For radiation reflected from relativistic electrons the Doppler factor on the denominator of equation (5.19) is negligibly small, and so our interference condition reduces to $\omega_\parallel \approx 2\pi l/d_\parallel$ (where l is an integer). If the separation distance in the laboratory frame is $d_\parallel = \lambda_0$, then constructive interference would only be detected at harmonics $\omega_\parallel = l\omega_0$, which is rapidly varying and of little physical use. However if the electron spacing is one wavelength in the rest frame λ_0/γ_0 or equivalently in the laboratory frame $d_\parallel = \lambda_0/\gamma_0^2$ as given by a Lorentz contraction, then the condition for constructive interference becomes $\omega_\parallel \approx l\gamma_0^2\omega_0$. Therefore we expect to see destructive interference at $l = 3.5$, constructive at $l = 4$ which corresponds to the Doppler reflected frequency $\omega_\parallel \approx 4\gamma_0^2\omega_0$, then destructive at $l = 4.5$ with some sinusoidal variation between these frequencies.

36

With the simulation completed we can consult Figure 5.3a, where both the case for one electron and two longitudinally separated electrons has been plotted for comparison. As predicted the peak at $\vartheta = \pi$ ($l = 4$) is exactly coherent, increasing compared to the one electron case with the number of particles squared, a factor of four. The peaks at angles $\vartheta = \pi + 1/4\gamma_0$ and $\vartheta = \pi + 1/2\gamma_0$ clearly experience some amplification but are not fully coherent; both are distorted by the destructive interference at $l = 3.5$ predicted above, which is not seen in the one electron case. In Figure 5.3b we see constructive interference with small angles at the Doppler reflected frequency, unlike the rapidly varying pattern we saw in Figure 5.2b.

This appears to suggest that by bunching many electrons longitudinally at this density, radiation emitted off axis will experience some destructive interference, producing a narrow / focused beam of light along the axis. Also, as radiation at off axis peaks tends to be at lower frequencies, the light produced is closer to being monochromatic. We should note that by increasing length L (5.24) which is equivalent to increasing the temporal profile of the pulse, one can produce light which is closer to being monochromatic, as one would expect from the uncertainty principle of the Fourier Transform.

(a) Variation with frequency.

(b) Variation with angle, at $\omega = 4\gamma_0^2\omega_0$.
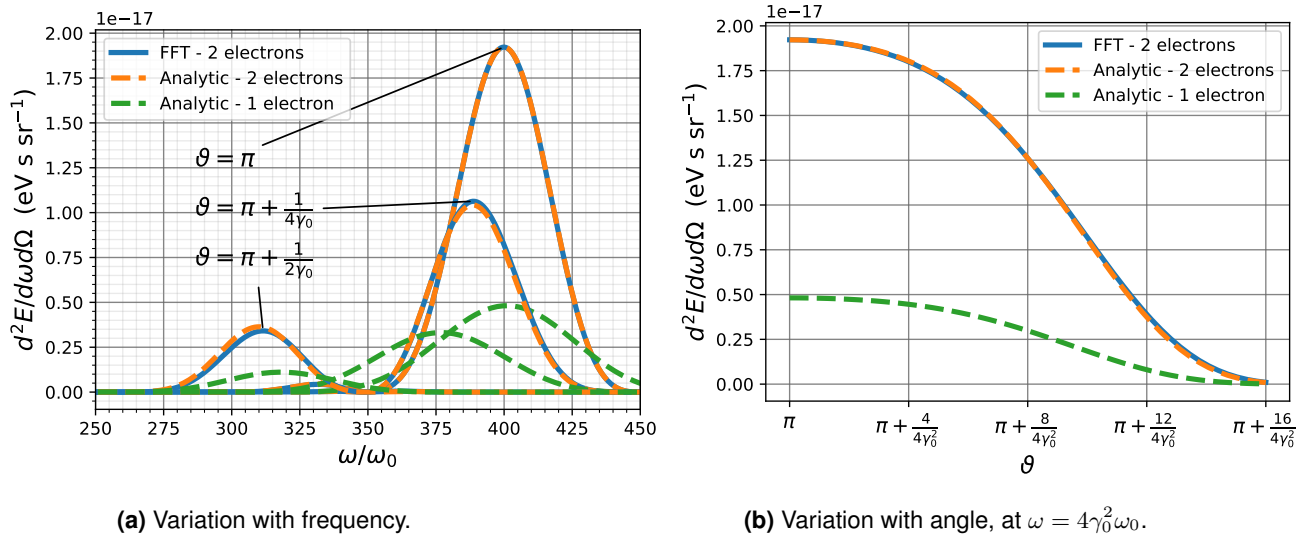
Figure 5.3: Energy radiated from two electrons with Lorentz factor $\gamma_0 = 10$, longitudinally separated by one wavelength, counter propagating with a plane wave pulse. Figure 5.3a shows the energy radiated varying with frequency, at specific angles within the radiation cone. Figure 5.3b shows the variation of energy radiated around the initial velocity, at the Doppler reflected frequency. ϑ is the angle between the observation direction and wave propagation direction, while $\vartheta = \pi$ is parallel to the initial velocity.

Chapter 6

Conclusion

In summary, we have successfully designed and tested a numerical code capable of modelling the spectrum and angular distribution of energy, radiated from some electron distribution. In addition, our code can model the spin precession of these electrons. This is contingent on the assumption that all electrons move with trajectories that can be independently determined, by an external field in the realm of classical electrodynamics.

In this thesis we initially explained the Runge-Kutta algorithms used by the code, and proceeded to test these in the case of a constant magnetic field. This was useful because exact analytic solutions could be derived for the electron trajectories, spin precession, and the spectrum of energy radiated from multiple electrons, which served as a useful benchmark for our code. By extending our analysis to a monochromatic plane wave, we were able to demonstrate that the electron spin should be unchanged after some integer number of oscillations providing small radiative corrections could be ignored. This idea, that an initially spin polarised electron beam will remain spin polarised, suggests that techniques such as laser wakefield acceleration could produce relativistic and focused spin polarised beams, as originally proposed by Wen, Tamburini and Keitel [WTK19].

For the case of two electrons with identical initial velocity interacting with a plane wave pulse of generic shape, we were able to define conditions for constructive interference (5.15). If the electron displacement, wave propagation direction and observation direction are all co-planar these condtions could be expressed in a simple format by equations (5.16) to (5.19). We must stress that these conditions have been derived assuming the observer is far away with respect to the electron trajectories, an assumption made in deriving the radiation integral (1.1). In the specific case of a linearly polarised plane wave pulse, these conditions were tested for separation of one wavelength transversely in the laboratory frame, and one wavelength longitudinally in the initial rest frame. Both simulations and approximate analytic solutions showed light emitted will be coherent parallel to the electron momentum, in the plane wave approximation for a far away observer. It appears that radiation from tightly bunched, longitudinally spaced electrons is coherent at small angles around the electron velocity, near the Doppler reflected frequency. If experimentally possible, the density of some electron pulse in the transverse and longitudinal directions could be tuned to produce coherent light, at a frequency determined by the electron momentum.

Having reviewed our key results, we can proceed to outline areas for improvement. This code could easily be extended to model radiative losses in the trajectory by applying the Runge-Kutta method to the Landau-Lifshitz equation [Di +12], which only becomes necessary when the energy

radiated during one oscillation is comparable to the initial electron energy. A more realistic laser pulse with a spatial and temporal profile could be employed to check if the interference conditions derived in this thesis are only appropriate in the plane wave approximation, or if they are more generally applicable. The speed of our numerical code is restricted by the numerical integration of the trajectories; a leapfrog scheme such as the Boris pusher could prove more effective when modelling large numbers of particles. If considering large particle numbers, one could extend our analysis to some Gaussian momentum distribution, instead of assuming all electrons have identical initial momentum. Furthermore, when deriving interference conditions we assumed all electrons propagated with the same initial momentum. By relaxing this assumption, it would be useful to derive an interference condition based on the initial momenta of the electrons.

Appendix A

Notation and Conventions

Units:

Throughout this thesis we use S.I. unit conventions, where $4\pi\varepsilon_0$ appears in the denominator of Coulomb's law, and natural units $\hbar = c = \varepsilon_0 = 1$, which are commonly found in high energy physics. In this choice of units the fine structure constant becomes $\alpha = e^2/4\pi \approx 1/137$. The electron has a charge of $-e$, mass m_e and anomalous electron magnetic moment $a_e = 1.159 \times 10^{-3}$. It is convenient to state the sign of the electron explicitly, as we often state the momentum, vector potential and fields relative to e and m_e.

Vector notation:

All vectors are denoted by bold typeface, e.g. $\boldsymbol{A}$, however this should also be obvious from context. Any vector denoted with a hat, e.g. $\hat{\boldsymbol{A}}$, is dimensionless and of unit length. A vector with a dot overhead represents the derivative of that vector function with respect to time $\dot{\boldsymbol{A}}(t)$. The Cartesian basis is referred to by $\hat{\boldsymbol{x}}$, $\hat{\boldsymbol{y}}$, $\hat{\boldsymbol{z}}$.

The electron position is $\boldsymbol{r}$, and the velocity is always stated in units of the speed of light c (which we have set equal to one) following the conventions of Jackson [Jac98],

$$\boldsymbol{\beta} = \frac{d\boldsymbol{r}}{dt} = \boldsymbol{v}. \tag{A.1}$$

We refer to the following dimensionless quantity as the momentum of an electron,

$$\boldsymbol{u} = \frac{d\boldsymbol{r}}{ds} = \gamma\boldsymbol{\beta}. \tag{A.2}$$

Where $ds^2 = c^2 dt^2 - dx^2 - dy^2 - dz^2$ is the world line of the particle in Minkowski space, with metric of signature $(+, -, -, -)$. The Lorentz factor is referred to interchangeably as a function of both velocity $\boldsymbol{\beta}$ and momentum $\boldsymbol{u}$,

$$\gamma(\beta) = \frac{1}{\sqrt{1 - \boldsymbol{\beta}^2}}, \qquad \gamma(u) = \sqrt{1 + \boldsymbol{u}^2}, \tag{A.3}$$

and both definitions are equivalent $\gamma(\beta) \equiv \gamma(u)$. Here the square of a vector refers to a dot

product with itself. If we refer to a vector without bold typeface, we simply mean the magnitude of the vector, $u = |\boldsymbol{u}|$, unless stated otherwise.

Fields and potentials:

We refer to the following quantity as the normalised vector potential

$$\boldsymbol{a} = \frac{e}{m_e}\boldsymbol{A}, \tag{A.4}$$

where $\boldsymbol{A}$ is the vector potential, used to determine the electric and magnetic fields (respectively);

$$\boldsymbol{E} = -\frac{\partial \boldsymbol{A}}{\partial t}, \qquad \boldsymbol{B} = \nabla_{\boldsymbol{r}} \times \boldsymbol{A}. \tag{A.5}$$

Symbol a_0 refers to the amplitude of the normalised vector potential, $a_0 = eA_0/m_e$, and A_0 is the amplitude of the vector potential. A strong field is defined as $a_0 >> 1$, and a weak field as $a_0 \ll 1$; if $a_0 \approx 1$ then an electron will go from rest to becoming relativistic in less than one cycle.

The canonical momentum for an electron is normally defined as,

$$\boldsymbol{P}_{can} = \boldsymbol{p} - e\boldsymbol{A}. \tag{A.6}$$

where $\boldsymbol{p} = m_e\boldsymbol{u}$ (A.2), however we prefer to normalise this relative to the electron mass,

$$\boldsymbol{U}_{can} = \boldsymbol{u} - \boldsymbol{a}. \tag{A.7}$$

Appendix B

Electron equations of motion in a plane wave

This appendix will present key results from the Hamilton-Jacobi method of finding equations of motion, for an electron in a plane wave. One can find this derivation in several textbooks such as Landau-Lifshitz volume 2 [LL75, § 47, problem 2] and papers by Salamin and Faisal [SF96], Sarachik and Schappert [SS70]. In practice we will follow the derivation by Salamin and Faisal [SF96] almost exactly. The reason for repeating their derivation here is because of the frequency with which we use these results, and to highlight the normalised notation used in our thesis. An introduction to the Hamilton-Jacobi method can be found in many textbooks on classical mechanics [LL82, § 47].

Finding equations of motion using the Hamilton-Jacobi method

Consider an electron in the presence of a plane wave. For frequency ω_0 its phase can be written as $\varphi(t) = \omega_0[t - \hat{\boldsymbol{n}}_0 \cdot \boldsymbol{r}_j(t)]$. Such a wave can be described by a normalised vector potential $\boldsymbol{a}(\varphi)$. The Hamilton-Jacobi Equation (HJE) can be written for an electron in the presence of a potential $\boldsymbol{a}(\varphi)$, not in the presence of any free charges, as [LL75, § 16, eq. 16.11]

$$\left(\frac{\partial S}{\partial t}\right)^2 - (\nabla S + \boldsymbol{a})^2 = 1. \tag{B.1}$$

Where the Hamilton principle function $S(\boldsymbol{r}(t), t)$ which usually has dimensions of [Energy][Time], has been normalised relative to $m_e c$ such that it now has units of [Length]. Usually we seek solutions of the form [LL75; SF96]

$$S(\boldsymbol{r}(t), t) = \boldsymbol{\alpha} \cdot \boldsymbol{r} + \beta c t + F(\varphi). \tag{B.2}$$

Where $\boldsymbol{\alpha}$ and β are dimensionless constants determined by the initial conditions, at some initial phase ϕ_0. Substitution of (B.2) into (B.1) and requiring the wave to be transverse $\hat{\boldsymbol{n}}_0 \cdot \boldsymbol{a}(\varphi) = 0$ in the Lorenz gauge yields an integral equation for F [SF96; SS70],

$$F(\varphi) = \frac{1}{2\omega_0} (\boldsymbol{\alpha} \cdot \hat{\boldsymbol{n}}_0 + \beta)^{-1} \int_{\phi_0}^{\varphi} \left(\boldsymbol{\alpha}^2 - \beta^2 + 1 + 2\boldsymbol{\alpha} \cdot \boldsymbol{a}(\varphi') + [\boldsymbol{a}(\varphi')]^2\right) d\varphi' \tag{B.3}$$

We have now solved for Hamilton's principle function $S(\varphi)$ (B.2). According to the general rules of the Hamilton-Jacobi method we differentiate the principle function with respect to the arbitrary constants $\boldsymbol{\alpha}$, and equate to new constants, which we choose to be the initial position $\nabla_{\boldsymbol{\alpha}} S = \boldsymbol{r}_0$ [SS70]

$$\omega_0(\boldsymbol{r}(\varphi) - \boldsymbol{r}(\phi_0)) = - \int_{\phi_0}^{\varphi} \frac{\boldsymbol{\alpha} + \boldsymbol{a}(\varphi')}{\boldsymbol{\alpha} \cdot \hat{\boldsymbol{n}}_0 + \beta} \, d\varphi' + \frac{\hat{\boldsymbol{n}}_0}{2} \int_{\phi_0}^{\varphi} \frac{\alpha^2 - \beta^2 + 1 + 2\boldsymbol{\alpha} \cdot \boldsymbol{a}(\varphi') + [\boldsymbol{a}(\varphi')]^2}{(\boldsymbol{\alpha} \cdot \hat{\boldsymbol{n}}_0 + \beta)^2} \, d\varphi'. \quad \text{(B.4)}$$

This is consistent with taking a canonical transformation to new co-ordinates $\boldsymbol{\alpha}$ and β [LL82]. Differentiating the principle function (B.2) with respect to the co-ordinates (B.4) allows us to obtain the canonical momentum $\nabla_{\boldsymbol{r}} S = \boldsymbol{U}_{can} = \boldsymbol{u} - \boldsymbol{a}$ (A.7), [SF96]

$$\boldsymbol{u}(\varphi) = \boldsymbol{\alpha} + \boldsymbol{a}(\varphi) - \frac{\hat{\boldsymbol{n}}_0}{2} \left(\frac{\alpha^2 - \beta^2 + 1 + 2\boldsymbol{\alpha} \cdot \boldsymbol{a}(\varphi) + [\boldsymbol{a}(\varphi)]^2}{\boldsymbol{\alpha} \cdot \hat{\boldsymbol{n}}_0 + \beta} \right). \quad \text{(B.5)}$$

Energy of the particle

Differentiating S with respect to time allows us to determine the Hamiltonian (or variable energy) stated in units of the rest mass energy $m_e c^2$ [SF96],

$$H(\varphi) = -\left(\beta + \hat{\boldsymbol{n}}_0 \cdot [\boldsymbol{\alpha} - \boldsymbol{U}_{can}(\varphi)] \right). \quad \text{(B.6)}$$

Where the $\boldsymbol{U}_{can}$ is the dimensionless canonical momentum (A.7). Using the transverse condition $\boldsymbol{a}(\varphi) \cdot \hat{\boldsymbol{n}}_0 = 0$ we can write this equivalently in terms of the momentum $\boldsymbol{u}$,

$$H(\varphi) = -\left(\beta + \hat{\boldsymbol{n}}_0 \cdot [\boldsymbol{\alpha} - \boldsymbol{u}(\varphi)] \right). \quad \text{(B.7)}$$

If we write down the usual (normalised to the rest mass energy) Hamiltonian for an electron in a plane wave, not in the presence of any free charges [LL75, § 16, eq. 16.10],

$$H(\varphi) = \sqrt{1 + (\boldsymbol{U}_{can}(\varphi) + \boldsymbol{a}(\varphi))^2} \equiv \sqrt{1 + [\boldsymbol{u}(\varphi)]^2} = \gamma(\varphi), \quad \text{(B.8)}$$

and compare equations (B.7) and (B.8), we can identify the following conserved quantity δ which appears throughout our equations of motion, eqs. (B.3) to (B.5),

$$\gamma(\varphi) - \hat{\boldsymbol{n}}_0 \cdot \boldsymbol{u}(\varphi) = -(\boldsymbol{\alpha} \cdot \hat{\boldsymbol{n}}_0 + \beta), \quad \text{(B.9)}$$

$$\Rightarrow \gamma_0 - \hat{\boldsymbol{n}}_0 \cdot \boldsymbol{u}_0 = \delta.$$

This conserved quantity is particularly useful as it allows us to determine a differential relationship between phase and time

$$\frac{d\varphi}{dt} = \omega_0 \left(1 - \frac{\hat{\boldsymbol{n}}_0 \cdot \boldsymbol{r}(t)}{c} \right) = \frac{\omega_0}{\gamma(\varphi)} \left(\gamma(\varphi) - \hat{\boldsymbol{n}}_0 \cdot \boldsymbol{u}(\varphi) \right) = \frac{\omega_0 \delta}{\gamma(\varphi)}. \quad \text{(B.10)}$$

43

Using this relationship (B.10) we can also find a simple differential relationship between the position and momentum (this is a generalised version of a result found by A. Macchi [Mac13, eqs. 2.26, 2.27])

$$\boldsymbol{u}(\varphi) = \gamma(t)\frac{d\boldsymbol{r}}{dt} = \gamma(\varphi)\frac{d\varphi}{dt}\frac{d\boldsymbol{r}}{d\varphi} = \delta\omega_0\frac{d\boldsymbol{r}}{d\varphi} \tag{B.11}$$

$$\omega_0(\boldsymbol{r}(\varphi) - \boldsymbol{r}_0) = \frac{1}{\delta}\int_{\phi_0}^{\varphi}\boldsymbol{u}(\varphi')d\varphi'. \tag{B.12}$$

These equations are entirely equivalent to those obtained earlier, eqs. (B.3) to (B.5).

Equations of motion in the laboratory frame

Constants α and β can be determined from the initial canonical momentum and position. Following Salamin and Faisal [SF96, section. B], we choose the normalised vector potential to be zero $\boldsymbol{a}(\phi_0) = 0$ in equation (B.5), which yields a relationship between constants α and β,

$$\boldsymbol{\alpha} = \boldsymbol{u}_0 - \frac{\hat{\boldsymbol{n}}_0}{2\delta}\left(\alpha^2 - \beta^2 + 1\right). \tag{B.13}$$

Without loss of generality we can choose $\boldsymbol{\alpha} = \boldsymbol{u}_0$ and $\beta = -\gamma_0$ (see [SF96, section B.] or [SS70, section A.]). The momentum can now be stated in its final form, in terms of the constant δ (B.9),

$$\boldsymbol{u}(\varphi) = \boldsymbol{u}_0 + \boldsymbol{a}(\varphi) + \frac{\hat{\boldsymbol{n}}_0}{\delta}\left(\boldsymbol{u}_0 \cdot \boldsymbol{a}(\varphi) + \frac{1}{2}[\boldsymbol{a}(\varphi)]^2\right) \tag{B.14}$$

The position of the particle is then given by integrating with respect to the phase, in (B.12).

Appendix C

Approximate solution of radiation integral in a weak, linearly polarised plane wave pulse

In this appendix we derive the energy radiated per unit solid angle, per unit frequency emitted from an arbitrary number of electrons counter propagating with a plane wave pulse. These particles are assumed to be moving ballistically, such that their motion is determined entirely from the external field.

Equations of motion

Consider the following plane wave pulse which is linearly polarised along $\hat{e}$ (A.4)

$$\boldsymbol{a}(\varphi) = \begin{cases} 0 & \text{for } \varphi < -L\pi, \\ a_0 \cos(\varphi) \cos^2\left(\frac{\varphi}{2L}\right) \hat{\boldsymbol{e}} & \text{for } -L\pi \leq \varphi \leq L\pi, \\ 0 & \text{for } L\pi < \varphi. \end{cases} \tag{C.1}$$

Parameter L determines the envelope half width, which we take as an integer to simplify our boundary terms when integrating. In this appendix we will always assume the normalised vector potential amplitude is small $a_0 \ll 1$, which we refer to as a weak field. The equation for momentum then becomes a perturbative expansion in a_0 (B.14). We are primarily interested in relativistic electrons counter propagating to the wave, so providing the following condition is valid,

$$|\boldsymbol{u}_{0,j} \cdot \hat{\boldsymbol{n}}_0| >> \frac{1}{2\delta_j} a_0^2, \tag{C.2}$$

we can ignore all terms proportional to a_0^2. Subscript j denotes a specific particle, so this condition must hold for all particles. $\delta_j = (\gamma_{0,j} - \hat{\boldsymbol{n}}_0 \cdot \boldsymbol{u}_{0,j})$ is a conserved quantity defined by equation (B.9). At $t = 0$, the initial position and momentum are determined at the initial phase $\phi_{0,j} = -\omega_0 \hat{\boldsymbol{n}}_0 \cdot \boldsymbol{r}_{0,j} < -L\pi$, where each particle starts outside the pulse. Ignoring terms of second order in the vector potential, we can write the particles' momenta as (B.14);

$$\boldsymbol{u}_j(\varphi) = \begin{cases} \boldsymbol{u}_{0,j} & \text{for } \phi_{0,j} \leq \varphi < -L\pi, \\ \boldsymbol{u}_{0,j} + a_0 \left(\hat{\boldsymbol{e}} + \frac{\hat{\boldsymbol{e}} \cdot \boldsymbol{u}_{0,j}}{\delta_j} \hat{\boldsymbol{n}}_0 \right) \cos(\varphi) \cos^2 \left(\frac{\varphi}{2L} \right) & \text{for } -L\pi \leq \varphi \leq L\pi, \\ \boldsymbol{u}_{0,j}, & \text{for } L\pi < \varphi. \end{cases} \tag{C.3}$$

Which can be integrated to find the trajectory (B.12), inside the pulse $-L\pi \leq \varphi \leq L\pi$,

$$\omega_0(\boldsymbol{r}_j(\varphi) - \boldsymbol{r}_{0,j}) = \frac{\boldsymbol{u}_{0,j}}{\delta_j}(\varphi - \phi_{0,j})$$
$$+ \frac{a_0}{4\delta_j} \left(\hat{\boldsymbol{e}} + \frac{\hat{\boldsymbol{e}} \cdot \boldsymbol{u}_{0,j}}{\delta_j} \hat{\boldsymbol{n}}_0 \right) \left(2\sin(\varphi) + \frac{\sin([1-L^{-1}]\varphi)}{1-L^{-1}} + \frac{\sin([1+L^{-1}]\varphi)}{1+L^{-1}} \right) \tag{C.4}$$

Using eqs. (C.3) and (C.4) we wish to solve for the spectrum of energy radiated by these electrons.

Solution to the radiation integral

The energy radiated is identically zero for any interval in which the momentum is constant (5.8), as expected. Equation (5.8) can be integrated by parts, without discarding the boundary terms, to obtain

$$\frac{d^2E}{d\omega d\Omega} = \frac{e^2}{16\pi^3} \left| \sum_j \left(\left[\frac{\hat{\boldsymbol{n}} \times (\hat{\boldsymbol{n}} \times \boldsymbol{u}_j(\varphi))}{\gamma_j(\varphi) - \hat{\boldsymbol{n}} \cdot \boldsymbol{u}_j(\varphi)} e^{i\Phi_j(\varphi)} \right]_{-\infty}^{\infty} - \frac{i\omega}{\delta_j\omega_0} \int_{-\infty}^{\infty} \hat{\boldsymbol{n}} \times (\hat{\boldsymbol{n}} \times \boldsymbol{u}_j(\varphi)) \, e^{i\Phi_j(\varphi)} d\varphi \right) \right|^2, \tag{C.5}$$

$$\Phi_j(\varphi) = \frac{\omega}{\omega_0} \left[\varphi + \omega_0(\hat{\boldsymbol{n}}_0 - \hat{\boldsymbol{n}}) \cdot \boldsymbol{r}_j(\varphi) \right]. \tag{C.6}$$

If we substitute the momentum (C.3) explicitly into the radiation integral (C.5), we can split our problem into three parts. Equation $\boldsymbol{K}_j$ (C.8) refers to the boundary terms from the integration by parts, $\boldsymbol{L}_j$ (C.9) refers to an integral over constant momentum, and $\boldsymbol{M}_j$ (C.10) refers to an integral over the normalised vector potential (C.1). Each electron's momentum is constant except in the interval $-L\pi \leq \varphi \leq L\pi$ (C.3), which we restrict our integration to.

$$\frac{d^2E}{d\omega d\Omega} = \frac{e^2}{16\pi^3} \left| \sum_j (\boldsymbol{K}_j + \boldsymbol{L}_j + \boldsymbol{M}_j) \right|^2, \tag{C.7}$$

$$\boldsymbol{K}_j = \left[\frac{\hat{\boldsymbol{n}} \times (\hat{\boldsymbol{n}} \times \boldsymbol{u}_j(\varphi))}{\gamma_j(\varphi) - \hat{\boldsymbol{n}} \cdot \boldsymbol{u}_j(\varphi)} e^{i\Phi_j(\varphi)} \right]_{-L\pi}^{L\pi}, \tag{C.8}$$

$$\boldsymbol{L}_j = -\frac{i\omega}{\delta_j\omega_0} \hat{\boldsymbol{n}} \times (\hat{\boldsymbol{n}} \times \boldsymbol{u}_{0,j}) \int_{-L\pi}^{L\pi} e^{i\Phi_j(\varphi)} d\varphi, \tag{C.9}$$

$$\boldsymbol{M_j} = -\frac{i\omega a_0}{\delta_j \omega_0} \left[\hat{\boldsymbol{n}} \times (\hat{\boldsymbol{n}} \times \hat{\boldsymbol{e}}) + \frac{\hat{\boldsymbol{e}} \cdot \boldsymbol{u}_{0,j}}{\delta_j} \hat{\boldsymbol{n}} \times (\hat{\boldsymbol{n}} \times \hat{\boldsymbol{n}}_0) \right] \int_{-L\pi}^{L\pi} \cos(\varphi) \cos^2\left(\frac{\varphi}{2L}\right) e^{i\Phi_j(\varphi)} d\varphi. \quad \text{(C.10)}$$

To solve these integrals, we need to define the phase term Φ_j by substituting our trajectory (C.4) into equation (C.6).

$$\Phi_j(\varphi) = \frac{\omega}{\omega_0} \left(\lambda_j + \sigma_j \varphi + 2\rho_j \sin(\varphi) + \frac{\rho_j}{1 + L^{-1}} \sin([1 + L^{-1}]\varphi) + \frac{\rho_j}{1 - L^{-1}} \sin([1 - L^{-1}]\varphi) \right). \quad \text{(C.11)}$$

Where Φ_j is determined in terms of the constants σ_j - a Doppler factor, λ_j - a constant depending on the j th particle's initial position and momentum, ρ_j - a parameter which determines the argument of our Bessel functions below. Each parameter depends on the initial electron momentum $\boldsymbol{u}_{0,j}$ and observation direction $\hat{\boldsymbol{n}}$:

$$\sigma_j = \frac{\gamma_{0,j} - \hat{\boldsymbol{n}} \cdot \boldsymbol{u}_{0,j}}{\gamma_{0,j} - \hat{\boldsymbol{n}}_0 \cdot \boldsymbol{u}_{0,j}} = \frac{1}{\delta_j} \left(\gamma_{0,j} - \hat{\boldsymbol{n}} \cdot \boldsymbol{u}_{0,j} \right), \quad \text{(C.12a)}$$

$$\lambda_j = \omega_0 (\sigma_j \hat{\boldsymbol{n}}_0 - \hat{\boldsymbol{n}}) \cdot \boldsymbol{r}_{0,j}, \quad \text{(C.12b)}$$

$$\rho_j = \frac{a_0}{4\delta_j} (\hat{\boldsymbol{n}}_0 - \hat{\boldsymbol{n}}) \cdot \left(\hat{\boldsymbol{e}} + \frac{\hat{\boldsymbol{e}} \cdot \boldsymbol{u}_{0,j}}{\delta_j} \hat{\boldsymbol{n}}_0 \right). \quad \text{(C.12c)}$$

We can exponentiate Φ_j this and re-write using the generating function, for Bessel functions of the first kind [AS64, eq. 9.1.41];

$$e^{\Phi_j(\varphi)} = e^{i\frac{\omega}{\omega_0}\lambda_j} \sum_{k,l,m=-\infty}^{\infty} J_k(x_k) J_l(x_l) J_m(x_m) \, e^{i\left[\frac{\omega}{\omega_0}\sigma_j + k + l(1+L^{-1}) + m(1-L^{-1})\right]\varphi} \quad \text{(C.13)}$$

$$x_k = 2\rho_j \frac{\omega}{\omega_0}, \qquad x_l = \frac{\rho_j}{1 + L^{-1}} \frac{\omega}{\omega_0}, \qquad x_m = \frac{\rho_j}{1 - L^{-1}} \frac{\omega}{\omega_0}. \quad \text{(C.14)}$$

Where x_k is the argument of Bessel function $J_k(x_k)$, but x_k does not actually vary with integer k, this is simply a short-hand notation.

We can start by solving the boundary terms $\boldsymbol{K}_j$ (C.8). Notice that the momentum (C.3) is unchanged from its initial value when the phase changes for integer multiples of π, $\boldsymbol{u}_{0,j} = \boldsymbol{u}_j(-L\pi) = \boldsymbol{u}_j(L\pi)$, this is also true for the Lorentz factor $\gamma_{0,j} = \sqrt{1 + \boldsymbol{u}_{0,j}^2}$ (A.3). The phase term (C.11) is not identical at both limits, $\Phi_j(-L\pi) = \omega(\lambda_j - L\pi\sigma_j)/\omega_0$ and $\Phi_j(L\pi) = \omega(\lambda_j + L\pi\sigma_j)/\omega_0$, which gives rise to a sinusoidal term. With this information we have determined $\boldsymbol{K}_j$ (C.8),

$$\boldsymbol{K_j} = 2i \, e^{i\frac{\omega}{\omega_0}\lambda_j} \sin\left(\frac{\omega}{\omega_0} \sigma_j L\pi \right) \frac{\hat{\boldsymbol{n}} \times (\hat{\boldsymbol{n}} \times \boldsymbol{u}_{0,j})}{\gamma_{0,j} - \hat{\boldsymbol{n}} \cdot \boldsymbol{u}_{0,j}} \quad \text{(C.15)}$$

By substituting the phase term (C.13) into our integral over constant momentum $\boldsymbol{L}_j$ (C.9) and solving, will result in equation (C.16) below. To obtain this, we separate out the term of order zero

47

$k = l = m = 0$, and re-arrange using the definitions of parameter σ_j (C.12a) and the conserved quantity δ_j (B.9).

$$\boldsymbol{L}_m = -2i\, e^{i\frac{\omega}{\omega_0}\lambda_j} \sin\left(\frac{\omega}{\omega_0}\sigma_j L\pi\right) \frac{\hat{\boldsymbol{n}} \times (\hat{\boldsymbol{n}} \times \boldsymbol{u}_{0,j})}{\gamma_{0,j} - \hat{\boldsymbol{n}} \cdot \boldsymbol{u}_{0,j}} J_0(x_k)J_0(x_l)J_0(x_m)$$

$$- \frac{i\omega}{\delta_j\omega_0} e^{i\frac{\omega}{\omega_0}\lambda_j} \hat{\boldsymbol{n}} \times (\hat{\boldsymbol{n}} \times \boldsymbol{u}_{0,j}) \sum_{\substack{k,l,m=-\infty, \\ k=l=m\neq 0.}}^{\infty} J_k(x_k)J_l(x_l)J_m(x_m)D_{k,l,m}(\omega), \quad \text{(C.16)}$$

where,

$$D_{k,l,m}(\omega) = 2L\pi\ \mathrm{sinc}\left(\left[\frac{\omega}{\omega_0}\sigma_j + k + l(1 + L^{-1}) + m(1 - L^{-1})\right]L\pi\right), \qquad \text{and}\ \ \mathrm{sinc}(x) = \frac{\sin(x)}{x}.$$
$$\text{(C.17)}$$

If we apply the usual plane wave approximation of sending the pulse length to infinity $\lim(L \to \infty)$, then D behaves like a Dirac delta function located at some frequency determined by the Doppler shift σ_j (C.12a).
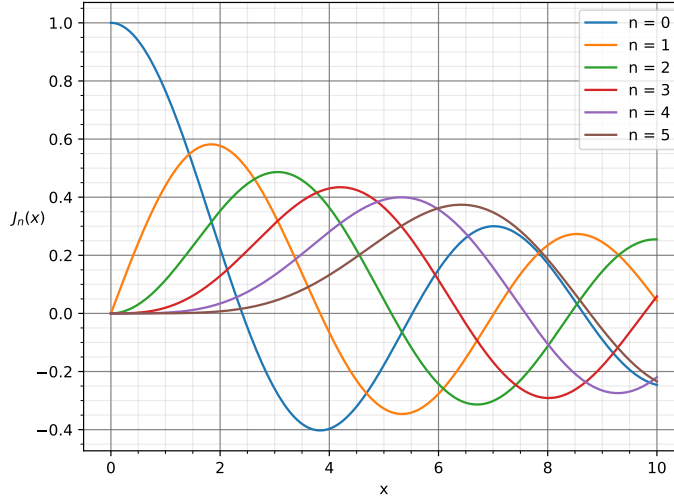
Figure C.1: Behaviour of Bessel functions of the first kind, integer order, for small arguments. Created using using Bessel function approximations from the Scipy.special package in Python [Vir+20].

Truncating the Bessel function series

Consider a relativistic electron initially counter propagating to the pulse with momentum $\boldsymbol{u}_{0,j} = -u_{0,j}\hat{\boldsymbol{n}}_0$ for $u_{0,j} >> 1$. Such an electron will have a value of $\delta_j \approx 2\gamma_{0,j}$. Most of the radiation will be emitted in a cone of full angle $1/\gamma_0$ around the momentum $\boldsymbol{u}_0$ [LL75, δ 73], near the Doppler shifted frequency $\omega \approx 4\gamma_0^2$. In this case ρ_j (C.12c) is approximately

$$\rho_j \approx -\frac{a_0\hat{\boldsymbol{n}} \cdot \hat{\boldsymbol{e}}}{8\gamma_{0,j}}. \tag{C.18}$$

Assuming the observation $\hat{n}$, polarisation $\hat{e}$ and wave propagation $\hat{n}_0$ are coplanar (as we expect for a linearly polarised pulse), it is clear the maximum value of ρ_j will be seen at the radiation cone edge, at angle $1/2\gamma_{0,j}$; using the small angle approximation we obtain $\hat{n} \cdot \hat{e} \approx 1/2\gamma_{0,j}$. Then we can estimate the maximum value of the argument of each Bessel function at frequency $\omega \approx 4\gamma_0^2$,

$$\left| \frac{\omega}{\omega_0} \rho_{j,max} \right| \approx \frac{a_0}{4}. \tag{C.19}$$

Providing the pulse is weak $a_0 \ll 1$, the argument of each Bessel function will be small within the radiation cone at these frequencies. Therefore the series of Bessel functions is perturbative and can be truncated at some point, and because the argument is assumed much smaller than one, we can assume the zero th order Bessel function is approximately one $J_0(x) \approx 1$ for $x \ll 1$ (see Figure C.1). If this approximation holds for each Bessel function, for each particle, then the zero order term $k = l = m = 0$ of $\boldsymbol{L}_j$ (C.16) and the boundary term $\boldsymbol{K}_j$ (C.8) cancel out. Adding $\boldsymbol{K}_j$ and $\boldsymbol{L}_j$, and using the following property of Bessel functions, $J_{-n}(x) = (-1)^n J_n(x)$, to remove negative indices we can obtain;

$$\boldsymbol{K}_j + \boldsymbol{L}_j \approx -\frac{i\omega}{\delta_j \omega_0} e^{i\frac{\omega}{\omega_0}\lambda_j} \hat{n} \times (\hat{n} \times \boldsymbol{u}_{0,j}) \sum_{\substack{k,l,m=-\infty, \\ k=l=m\neq 0.}}^{\infty} J_k(x_k) J_l(x_l) J_m(x_m) \left[D_{k,l,m}(\omega) \right.$$

$$\left. + (-1)^{k+l+m} D_{-k,-l,-m}(\omega) \right]. \tag{C.20}$$

The approximation in equation (C.20) usually holds well for long pulses $L \gg 1$, as the terms which cancel do not scale with L. Now consider the second integral $\boldsymbol{M}_j$ (C.10), over the oscillating momentum component. Substituting in $\exp(i\Phi_j)$ (C.13) and ignoring the constant prefactor of $\boldsymbol{M}_j$, we obtain,

$$\int_{-L\pi}^{L\pi} \cos(\varphi) \cos^2\left(\frac{\varphi}{2L}\right) e^{i\Phi_j(\varphi)} d\varphi$$

$$= e^{i\frac{\omega}{\omega_0}\lambda_j} \int_{-L\pi}^{L\pi} e^{i\frac{\omega}{\omega_0}\sigma_j\varphi} \sum_{k,l,m=-\infty}^{\infty} \cos(\varphi) \cos^2\left(\frac{\varphi}{2L}\right) J_k(x_k) J_l(x_l) J_m(x_m) e^{i\left[k+l(1+L^{-1})+m(1-L^{-1})\right]\varphi} .d\varphi. \tag{C.21}$$

If we expand out the sinusoid as a series of phase terms;

$$\cos(\varphi) \cos^2\left(\frac{\varphi}{2L}\right) = \frac{1}{4}\left(e^{i\varphi} + e^{-i\varphi}\right) + \frac{1}{8}\left(e^{i[1+L^{-1}]\varphi} + e^{i[1-L^{-1}]\varphi} + e^{-i[1-L^{-1}]\varphi} + e^{-i[1+L^{-1}]\varphi}\right), \tag{C.22}$$

we can see that by shifting the sum indices we can replace these oscillatory terms with Bessel functions; for example the first term can be removed by translating $k \rightarrow k-1$. We can then combine the resulting series of Bessel functions using the recurrence relation $2n J_n(x)/x = J_{n-1}(x) + J_{n+1}(x)$ [AS64, pg. 361, 9.1.27] repeatedly. Finally the sum inside the integrand of equation (C.21) becomes,

$$\frac{1}{2} \sum_{k,l,m=-\infty}^{\infty} \left(\frac{k}{x_k} + \frac{1}{2} \left[\frac{l}{x_l} + \frac{m}{x_m} \right] \right) J_k(x_k) J_l(x_l) J_m(x_m) \; e^{i\left[k+l(1+L^{-1})+m(1-L^{-1}) \right]\varphi}. \tag{C.23}$$

Note the zero th order term $k = l = m = 0$ is identically zero. Substituting this sum (C.23) in place of the sum in equation (C.21) and integrating produces

$$\int_{-L\pi}^{L\pi} \cos(\varphi) \cos^2\left(\frac{\varphi}{2L} \right) \; e^{i\Phi_j(\varphi)} d\varphi$$

$$= \frac{1}{2} e^{i\frac{\omega}{\omega_0}\lambda_j} \sum_{k,l,m=0}^{\infty} \left(\frac{k}{x_k} + \frac{1}{2} \left[\frac{l}{x_l} + \frac{m}{x_m} \right] \right) J_k(x_k) J_l(x_l) J_m(x_m) \left[D_{k,l,m}(\omega) - (-1)^{k+l+m} D_{-k,-l,-m}(\omega) \right].$$

$$\tag{C.24}$$

Where function $D_{k,l,m}$ (C.17) has already been referred to. Combining our equation for $\boldsymbol{K}_j + \boldsymbol{L}_j$ (C.20) and substituting the result above (C.24) into our equation for $\boldsymbol{M}_j$ (C.10), one can obtain the complete expression;

$$\boldsymbol{K}_j + \boldsymbol{L}_j + \boldsymbol{M}_j \approx$$

$$\frac{\omega}{\delta_j \omega_0} e^{i\frac{\omega}{\omega_0}\lambda_j} \left\{ \sum_{\substack{k,l,m=0, \\ k=l=m\neq 0.}}^{\infty} J_k(x_k) J_l(x_l) J_m(x_m) \left(\hat{\boldsymbol{n}} \times (\hat{\boldsymbol{n}} \times \boldsymbol{u}_{0,j}) \left[D_{k,l,m}(\omega) + (-1)^{k+l+m} D_{-k,-l,-m}(\omega) \right] \right. \right.$$

$$\left. \left. + \frac{a_0}{2} \left[\hat{\boldsymbol{n}} \times (\hat{\boldsymbol{n}} \times \hat{\boldsymbol{e}}) + \frac{\hat{\boldsymbol{e}} \cdot \boldsymbol{u}_{0,j}}{\delta_j} \hat{\boldsymbol{n}} \times (\hat{\boldsymbol{n}} \times \hat{\boldsymbol{n}}_0) \right] \left[\frac{k}{x_k} + \frac{1}{2} \left(\frac{l}{x_l} + \frac{m}{x_m} \right) \right] \left[D_{k,l,m}(\omega) - (-1)^{k+l+m} D_{-k,-l,-m}(\omega) \right] \right) \right\}$$

$$\tag{C.25}$$

Any factors which vanish under the square modulus (C.7) have been discarded. We have previously assumed the Bessel function arguments are small, so it is natural to truncate this series. Simply truncating the series for order zero $k = l = m = 0$ would obtain a null result in our approximation. So far we have assumed $J_0(x) \approx 1$ for $x \ll 1$, and we expect higher order terms to converge rapidly to zero from Figure C.1. A simple choice is to truncate this series for terms that satisfy $k + l + m = 1$. It may help to first expand Bessel functions divided by their argument using the recurrence relation,

$$\frac{n J_n(x)}{x} = \frac{1}{2} \left(J_{n-1}(x) + J_{n+1}(x) \right), \tag{C.26}$$

such that $J_1(x)/x \approx 1/2$ for $x \ll 1$. The full solution is stated below in equation (C.27). We have tried to state as many quantities as possible explicitly, by including the arguments of any Bessel functions (C.14), and the sinc functions (C.17). Substituting the equation below for $\boldsymbol{K}_j + \boldsymbol{L}_j + \boldsymbol{M}_j$ into equation (C.7) will give a general expression for the energy radiated by an arbitrary number of particles, per unit solid angle, per unit frequency. Expanding out the square modulus even for a single particle can be cumbersome, so in practice we have written a Python script to evaluate this. Our answer is still stated in terms of the Doppler factor σ_j (C.12a) and constant λ_j which contains information about the electron's initial position (C.12b).

50

$$
\boldsymbol{K}_j + \boldsymbol{L}_j + \boldsymbol{M}_j \approx \frac{2L\pi\omega}{\delta_j\omega_0} e^{i\frac{\omega}{\omega_0}\lambda_j} \Bigg\{
$$

$$
\hat{\boldsymbol{n}} \times (\hat{\boldsymbol{n}} \times \boldsymbol{u}_{0,j}) \Bigg(J_1\Big(2\rho_j\frac{\omega}{\omega_0}\Big) \bigg[\mathrm{sinc}\left(\Big[\frac{\omega}{\omega_0}\sigma_j + 1\Big]L\pi\right) - \mathrm{sinc}\left(\Big[\frac{\omega}{\omega_0}\sigma_j - 1\Big]L\pi\right) \bigg]
$$

$$
+ J_1\Big(\frac{\omega\rho_j}{\omega_0(1+L^{-1})}\Big) \bigg[\mathrm{sinc}\left(\Big[\frac{\omega}{\omega_0}\sigma_j + 1 + L^{-1}\Big]L\pi\right) - \mathrm{sinc}\left(\Big[\frac{\omega}{\omega_0}\sigma_j - 1 - L^{-1}\Big]L\pi\right) \bigg]
$$

$$
+ J_1\Big(\frac{\omega\rho_j}{\omega_0(1-L^{-1})}\Big) \bigg[\mathrm{sinc}\left(\Big[\frac{\omega}{\omega_0}\sigma_j + 1 - L^{-1}\Big]L\pi\right) - \mathrm{sinc}\left(\Big[\frac{\omega}{\omega_0}\sigma_j - 1 + L^{-1}\Big]L\pi\right) \bigg] \Bigg)
$$

$$
+ \frac{a_0}{4} \bigg[\hat{\boldsymbol{n}} \times (\hat{\boldsymbol{n}} \times \hat{\boldsymbol{e}}) + \frac{\hat{\boldsymbol{e}} \cdot \boldsymbol{u}_{0,j}}{\delta_j} \hat{\boldsymbol{n}} \times (\hat{\boldsymbol{n}} \times \hat{\boldsymbol{n}}_0) \bigg] \bigg[\mathrm{sinc}\left(\Big[\frac{\omega}{\omega_0}\sigma_j + 1\Big]L\pi\right) + \mathrm{sinc}\left(\Big[\frac{\omega}{\omega_0}\sigma_j - 1\Big]L\pi\right)
$$

$$
+ \frac{1}{2}\mathrm{sinc}\left(\Big[\frac{\omega}{\omega_0}\sigma_j + 1 + L^{-1}\Big]L\pi\right) + \frac{1}{2}\mathrm{sinc}\left(\Big[\frac{\omega}{\omega_0}\sigma_j - 1 - L^{-1}\Big]L\pi\right)
$$

$$
+ \frac{1}{2}\mathrm{sinc}\left(\Big[\frac{\omega}{\omega_0}\sigma_j + 1 - L^{-1}\Big]L\pi\right) + \frac{1}{2}\mathrm{sinc}\left(\Big[\frac{\omega}{\omega_0}\sigma_j - 1 + L^{-1}\Big]L\pi\right) \bigg] \Bigg\}
$$

$$
(\text{C.27})
$$

Bibliography

[Ada+13]   Bernhard W. Adams et al. "X-ray quantum optics". In: *Journal of Modern Optics* 60.1 (Jan. 2013), pp. 2–21. DOI: 10.1080/09500340.2012.752113. eprint: https://doi.org/10.1080/09500340.2012.752113.

[Ama+12]   J. Amann et al. "Demonstration of self-seeding in a hard-X-ray free-electron laser". In: *Nature Photonics* 6.10 (Oct. 2012), pp. 693–698. ISSN: 1749-4893. DOI: 10.1038/nphoton.2012.180.

[AS64]   Milton Abramowitz and Irene A. Stegun. *Handbook of Mathematical Functions with Formulas, Graphs, and Mathematical Tables.* ninth Dover printing, tenth GPO printing. New York City: Dover, 1964.

[BET03]   Sergei V. Bulanov, Timur Esirkepov, and Toshiki Tajima. "Light Intensification towards the Schwinger Limit". In: *Phys. Rev. Lett.* 91 (8 Aug. 2003), p. 085001. DOI: 10.1103/PhysRevLett.91.085001.

[BMT59]   V. Bargmann, Louis Michel, and V. L. Telegdi. "Precession of the Polarization of Particles Moving in a Homogeneous Electromagnetic Field". In: *Phys. Rev. Lett.* 2 (10 May 1959), pp. 435–436. DOI: 10.1103/PhysRevLett.2.435.

[BPL82]   V.B. Berestetskii, L.P. Pitaevskii, and E.M. Lifshitz. *Quantum Electrodynamics (Landau and Lifshitz Course of Theoretical Physics, vol. 4, 2nd edition).* Elsevier Science, 1982. ISBN: 9780080503462.

[Bul+13]   Sergei V Bulanov et al. "Relativistic mirrors in plasmas. Novel results and perspectives". In: *Physics-Uspekhi* 56.5 (May 2013), pp. 429–464. DOI: 10.3367/ufne.0183.201305a.0449.

[Col+16]   Jacques-Philippe Colletier et al. "De novo phasing with X-ray laser reveals mosquito larvicide BinAB structure". In: *Nature* 539.7627 (Nov. 2016), pp. 43–47. ISSN: 1476-4687. DOI: 10.1038/nature19825.

[CT65]   J. Cooley and John W. Tukey. "An algorithm for the machine calculation of complex Fourier series". In: *Mathematics of Computation* 19 (1965), pp. 297–301. DOI: 10.1090/S0025-5718-1965-0178586-1.

[Dal+11]   Lisandro D. Dalcin et al. "Parallel distributed computing using Python". In: *Advances in Water Resources* 34.9 (2011). New Computational Methods and Software Tools, pp. 1124–1139. ISSN: 0309-1708. DOI: https://doi.org/10.1016/j.advwatres.2011.04.013.

[Di +12]   A. Di Piazza et al. "Extremely high-intensity laser interactions with fundamental quantum systems". In: *Rev. Mod. Phys.* 84 (3 Aug. 2012), pp. 1177–1228. DOI: 10.1103/RevModPhys.84.1177.

[Dro+06]   B. Dromey et al. "High harmonic generation in the relativistic limit". In: *Nature Physics* 2.7 (July 2006), pp. 456–459. ISSN: 1745-2481. DOI: 10.1038/nphys338.

[Edw+94]   Glenn Edwards et al. "Tissue ablation by a free-electron laser tuned to the amide II band". In: *Nature* 371.6496 (Sept. 1994), pp. 416–419. ISSN: 1476-4687. DOI: 10.1038/371416a0.

[Ein05]   A. Einstein. "Zur Elektrodynamik bewegter Körper". In: *Annalen der Physik* 322.10 (1905), pp. 891–921. DOI: 10.1002/andp.19053221004.

[Emm+10]   P. Emma et al. "First lasing and operation of an ångstrom-wavelength free-electron laser". In: *Nature Photonics* 4.9 (Sept. 2010), pp. 641–647. ISSN: 1749-4893. DOI: 10.1038/nphoton.2010.176.

[ESL09]   E. Esarey, C. B. Schroeder, and W. P. Leemans. "Physics of laser-driven plasma-based electron accelerators". In: *Rev. Mod. Phys.* 81 (3 Aug. 2009), pp. 1229–1285. DOI: 10.1103/RevModPhys.81.1229.

[Har+20]   Charles R. Harris et al. "Array programming with NumPy". In: *Nature* 585 (2020), pp. 357–362. DOI: 10.1038/s41586-020-2649-2.

[Jac98]   John David Jackson. *Classical Electrodynamics, 3rd Edition*. Wiley, 1998.

[KI09]   Ferenc Krausz and Misha Ivanov. "Attosecond physics". In: *Rev. Mod. Phys.* 81 (1 Feb. 2009), pp. 163–234. DOI: 10.1103/RevModPhys.81.163.

[KKP09]   Jens Keiner, Stefan Kunis, and Daniel Potts. "Using NFFT 3—A Software Library for Various Nonequispaced Fast Fourier Transforms". In: *ACM Trans. Math. Softw.* 36.4 (Aug. 2009). ISSN: 0098-3500. DOI: 10.1145/1555386.1555388.

[Kor+18]   Dmitrii Kormin et al. "Spectral interferometry with waveform-dependent relativistic high-order harmonics from plasma surfaces". In: *Nature Communications* 9.1 (Nov. 2018), p. 4992. ISSN: 2041-1723. DOI: 10.1038/s41467-018-07421-5.

[LCL]   LCLS. *Linac Coherent Light Source*. https://lcls.slac.stanford.edu/. Accessed: 20 October 2020.

[LL75]   L. D. Landau and E. M. Lifshitz. *The Classical Theory of Fields*. Fourth Revised English Edition. Vol. 2. Course of Theoretical Physics. Amsterdam: Pergamon, 1975. ISBN: 978-0-08-025072-4. DOI: 10.1016/B978-0-08-025072-4.50005-8.

[LL82]   L. D. Landau and E. M. Lifshitz. *Mechanics*. Third Edition. Course of Theoretical Physics. Pergamon, 1982. ISBN: 9780750628969.

[LPS15]   Siu Kwan Lam, Antoine Pitrou, and Stanley Seibert. "Numba: A LLVM-Based Python JIT Compiler". In: LLVM '15 (2015). DOI: 10.1145/2833157.2833162.

[Mac13]   Andrea Macchi. *A Superintense Laser-Plasma Interaction Theory Primer*. SpringerBriefs in Physics. Springer Netherlands, 2013. ISBN: 9789400761254. DOI: 10.1103/PhysRevLett.2.435.

[Neu+00]   Richard Neutze et al. "Potential for biomolecular imaging with femtosecond X-ray pulses". In: *Nature* 406.6797 (Aug. 2000), pp. 752–757. ISSN: 1476-4687. DOI: 10.1038/35021099.

[Pia08]   A. Di Piazza. "Exact Solution of the Landau-Lifshitz Equation in a Plane Wave". In: *Letters in Mathematical Physics* 83.3 (Mar. 2008), pp. 305–313. ISSN: 1573-0530. DOI: 10.1007/s11005-008-0228-9.

[Pre+92]   William H. Press et al. *Numerical Recipes in FORTRAN (2nd Ed.): The Art of Scientific Computing*. Cambridge University Press, 1992. ISBN: 052143064X.

[PS95]   Michael E. Peskin and Daniel V. Schroeder. *An Introduction to quantum field theory*. Reading, USA: Addison-Wesley, 1995. ISBN: 978-0-201-50397-5.

[Pyt19]   Python. *Documentation for Python 3.7.4*. https://docs.python.org/3.7/. Accessed: 13 October 2020. July 2019.

[RHB06]   K. F. Riley, M. P. Hobson, and S. J. Bence. *Mathematical Methods for Physics and Engineering: A Comprehensive Guide*. Cambridge University Press, 2006.

[RK10]   Brian Reville and John G. Kirk. "COMPUTATION OF SYNTHETIC SPECTRA FROM SIMULATIONS OF RELATIVISTIC SHOCKS". In: *The Astrophysical Journal* 724.2 (Nov. 2010), pp. 1283–1295. DOI: 10.1088/0004-637x/724/2/1283.

[Sam+20]   Archana Sampath et al. *Extremely Dense Gamma-Ray Pulses in Electron Beam-Multifoil Collisions*. 2020. arXiv: 2009.01808 [physics.plasm-ph].

[Sch+13]   B. S. Schlimme et al. "Measurement of the Neutron Electric to Magnetic Form Factor Ratio at $Q^2{=}1.58\ \mathrm{GeV}^2$ Using the Reaction $^3\vec{\mathrm{He}}\,(\vec{e},e^{'}n)pp$". In: *Phys. Rev. Lett.* 111 (13 Sept. 2013), p. 132504. DOI: 10.1103/PhysRevLett.111.132504.

[Sch49]   Julian Schwinger. "On the Classical Radiation of Accelerated Electrons". In: *Phys. Rev.* 75 (12 June 1949), pp. 1912–1925. DOI: 10.1103/PhysRev.75.1912.

[SF96]   Yousef I. Salamin and Farhad H. M. Faisal. "Harmonic generation by superintense light scattering from relativistic electrons". In: *Phys. Rev. A* 54 (5 Nov. 1996), pp. 4383–4395. DOI: 10.1103/PhysRevA.54.4383.

[Sin+16]   A. Singer et al. "Photoinduced Enhancement of the Charge Density Wave Amplitude". In: *Phys. Rev. Lett.* 117 (5 July 2016), p. 056401. DOI: 10.1103/PhysRevLett.117.056401.

[SS70]   E. S. Sarachik and G. T. Schappert. "Classical Theory of the Scattering of Intense Laser Radiation by Free Electrons". In: *Phys. Rev. D* 1 (10 May 1970), pp. 2738–2753. DOI: 10.1103/PhysRevD.1.2738.

[Tol56]   H. A. Tolhoek. "Electron Polarization, Theory and Experiment". In: *Rev. Mod. Phys.* 28 (3 July 1956), pp. 277–298. DOI: 10.1103/RevModPhys.28.277.

[Van17]   Jake VanderPlas. *Python wrapper for the non-equispaced fast Fourier transform (NFFT), v0.1*. https://github.com/jakevdp/nfft. Accessed: 13 October 2020. Apr. 2017.

[Vir+20]   Pauli Virtanen et al. "SciPy 1.0: Fundamental Algorithms for Scientific Computing in Python". In: *Nature Methods* 17 (2020), pp. 261–272. DOI: 10.1038/s41592-019-0686-2.

[Wie+18]   Max O. Wiedorn et al. "Megahertz serial crystallography". In: *Nature Communications* 9.1 (Oct. 2018), p. 4025. ISSN: 2041-1723. DOI: 10.1038/s41467-018-06156-7.

[WTK19]   Meng Wen, Matteo Tamburini, and Christoph H. Keitel. "Polarized Laser-WakeField-Accelerated Kiloampere Electron Beams". In: *Phys. Rev. Lett.* 122 (21 May 2019), p. 214801. DOI: 10.1103/PhysRevLett.122.214801.

[XFE]   XFEL. *Eureopan X-ray Free Electron Laser*. https://www.xfel.eu/. Accessed: 20 October 2020.

Acknowledgments

I wish to thank my supervisors Dr. Matteo Tamburini and P.D. Dr. Antonino Di Piazza, whose guidance was essential for completing this thesis, as well as P.D. Dr. Robert Moshammer who agreed to be the secondary examiner of this thesis. Furthermore I am grateful for the facilities and computing resources provided by the Max Planck Institute for Nuclear Physics (MPI-K), specifically by the division of Honorarprofessor Christoph Keitel. I would also like to express my gratitude towards Dr. Halil Cakir who assisted me with the translation of my abstract into German. Finally, I appreciate many fruitful discussions with fellow students at MPI-K; specifically Kamil Dzikowski, Daniel Bakucz Canário, Petar Andrejic, Igor Valuev and Archana Sampath.

Declaration

I declare that I wrote this thesis myself, and did not use any sources other than those stated.

Heidelberg, 29 October 2020, Michael John Quin.

Please see the next page for the signed, authoritative declaration in German.

Erklärung:

Ich versichere, dass ich diese Arbeit selbstständig verfasst habe und keine anderen als die angegebenen Quellen und Hilfsmittel benutzt habe.

Heidelberg, den (Datum)

29 Oktober 2020
....

Michael John Quin.